Anticancer Potential of Diiron Vinyliminium Complexes

Dalila Rocco,[a] Lucinda K. Batchelor,[b] Gabriele Agonigi,[a] Simona Braccini,[a] Federica Chiellini,[a] Silvia Schoch,[a] Tarita Biver,[d] Tiziana Funaioli,[a] Stefano Zacchini,[c] Lorenzo Biancalana,[a] Marina Ruggeri,[a] Guido Pampaloni,[a] Paul J. Dyson,[b,] Fabio Marchetti [a,*]*

[a] *Dipartimento di Chimica e Chimica Industriale, Università di Pisa, Via G. Moruzzi 13, I-56124 Pisa, Italy.*

[b] *Institut des Sciences et Ingénierie Chimiques, Ecole Polytechnique Fédérale de Lausanne (EPFL), CH-1015 Lausanne, Switzerland.*

[c] *Dipartimento di Chimica Industriale "Toso Montanari", Università di Bologna, Viale Risorgimento 4, I-40136 Bologna, Italy.*

[d] *Dipartimento di Farmacia, Università di Pisa, Via Bonanno 6, I-56126 Pisa, Italy.*

Corresponding Authors

*E-mail addresses:

fabio.marchetti1974@unipi.it (webpage: http://people.unipi.it/fabio_marchetti1974/), paul.dyson@epfl.ch

Abstract

Although ferrocene derivatives have attracted considerable attention as possible anticancer agents, the medicinal potential of diiron complexes has remained largely unexplored. Herein, we describe the straightforward multigram-scale synthesis and the antiproliferative activity of a series of diiron cyclopentadienyl complexes containing bridging vinyliminium ligands. IC_{50} values in the low to mid-micromolar range were determined against cisplatin sensitive and resistant human ovarian carcinoma (A2780 and A2780cisR) cell lines. Notable selectivity towards the cancerous cells lines compared to the non-tumoural human embryonic kidney (HEK-293) cell line was observed for selected compounds. The activity seems to be multimodal, involving ROS generation and, in some cases, a fragmentation process to afford monoiron derivatives. The large structural variability, amphiphilic character and good stability in aqueous media of the diiron vinyliminium complexes collectively provide favourable properties compared to other widely studied classes of iron-based anticancer candidates.

Keywords: bioorganometallic chemistry, metal-based drugs, diiron complexes, vinyliminium ligand, cytotoxicity.

Introduction

The peculiar characteristics of transition metals, including the variety of accessible redox states and coordination sites, offer a degree of structural diversity to metal-based drugs that is inaccessible to organic molecules.[1] Cisplatin and its derivatives are currently employed in the first line treatment of a wide range of cancers, but despite their unquestionable efficacy, severe side effects and progressive acquisition of drug resistance are associated with their use.[2,3] Consequently, a substantial effort has been focused on the development of alternative metal-based anticancer drugs with the ability to overcome the limitations of platinum-based chemotherapics.[4] In addition to alternative platinum-based

pharmaceuticals with enhanced properties,[5] complexes containing, among the others, titanium,[6] ruthenium,[7] gold [8] and iridium [8e,9] ions have been explored. However, several of the proposed compounds exhibit undesirable features such as low stability leading to the rapid substitution of ligands and poor water solubility. Indeed, stability in physiological media within a reasonable timeframe and an appropriate balance between water solubility and lipophilicity,[10] the latter favouring tumour tissue penetration and cellular uptake,[11] are important factors. In some cases, limited ligand exchange, e.g. where chloride ligands are replaced by water molecules, is key to the activation of the drug.[12] Instead, extensive degradation of a complex in biological medium could lead to fragments or aggregates which lack a clear pharmacological role.[13] The titanium complexes budotitane and titanocene dichloride failed clinical trials for reasons that are imputable to these drawbacks,[6b] while the ruthenium(III) complex KP1019 7[a] and the platinum(II) complex cis-dichlorobis(cyclopentylamine)platinum(II)[14] were limited by their poor water solubility.

As a bio-essential, relatively non-toxic element for which transport and storage mechanisms exist, iron is an appealing element for a metal-based drug.[15] Several monoiron complexes, including iron(II) cyclopentadienyl complexes,[16] have been investigated for their anticancer behaviour, and functionalized ferrocenes have emerged as promising candidates.[17,18] For example, a series of ferrocifens, constituted by the ferrocene unit bearing hydroxytamoxifen-type substituents on one of the two cyclopentadienyl rings, display significant cytotoxicity against a panel of cancer cell lines, which was attributed to a synergic effect between the organic moiety and the iron centre.[19a] The redox chemistry of the Fe(II) centre is believed to be an influential factor in the cytotoxicity of these compounds, as the oxidation to Fe(III) inside the cancer cell generates reactive metabolites and triggers the production of toxic substances.[19b,20] However, ferrocifens usually possess insufficient water solubility and consequently must be carefully formulated for potential clinical applications.[21]

The anticancer properties of diiron complexes are substantially unexplored, despite the opportunity of cooperative effects between the two metal centres and multisite coordination modes available to the ligands.[22] Hence, reactivity patterns that are not viable for mononuclear species may be accessible with dinuclear complexes giving rise to diverse structural motifs and physico-chemical properties.[23] It is worth mentioning that nature selected diiron carbonyl units as the catalytic core of some highly efficient enzymes.[24]

$Fe_2Cp_2(CO)_4$ (Cp = C_5H_5) is a classical starting compound in organometallic synthesis, enabling the preparation of unusual molecular architectures through sequential regio- and stereo-selective reactions.[25] Herein, we report a series of diiron complexes with a bridging vinyliminium ligand as a novel family of cytotoxic organometallic compounds (Figure 1). The complexes can be obtained on gram scales from $Fe_2Cp_2(CO)_4$ via the stepwise assembly of isocyanide and alkyne units,[25a] and display acceptable water solubility and stability. Spectro-electrochemical studies, ROS analysis and investigations on the interaction with biomolecules have been conducted to ascertain a possible mode of action.

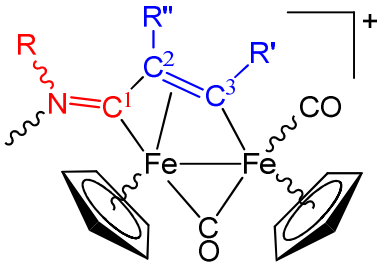

Figure 1. General structure of diiron μ-vinyliminium complexes obtained from the assembly of one isocyanide (fragment in red colour) and one alkyne (fragment in blue colour), starting from $Fe_2Cp_2(CO)_4$.

Results and discussion

1. Synthesis and characterization of compounds

The vinyliminium complexes [**2-19**]CF_3SO_3 were prepared from $Fe_2Cp_2(CO)_4$ following a four-step procedure (Scheme 1). The aminocarbyne precursors [**1a-c**]CF_3SO_3 were obtained via carbon monoxide/isocyanide substitution and subsequent alkylation in near quantitative yields (Scheme 1, steps 1-2).[26] One carbonyl ligand is subsequently replaced by a more labile acetonitrile molecule, which allows the entry and insertion of the alkyne into the iron-carbyne bond, forming the vinyliminium ligand (Scheme 1, steps 3-4). The last two steps were conducted using optimised literature procedures.[27] The alkyne insertion reaction (step 4) is tolerant of various hetero-functional groups, e.g. thiophenyl and pyridyl, despite their affinity for iron coordination:[28] the resulting vinyliminium ligands are reported here for the first time. The final complexes [**2-19**]CF_3SO_3, synthesised at ambient temperature and purified via chromatography without the need of an inert atmosphere, were isolated in good to high yields (52-96%) as air stable solid materials. Concerning the choice of the counteranion, it should be noted that a variety of ionic metal complexes with triflate as counteranion have been proposed to date as possible anticancer drugs,[29] and, among them, Ru(II) arene complexes with bidentate *N,N*-ligands were investigated in vivo showing no significant toxicity.[29b]

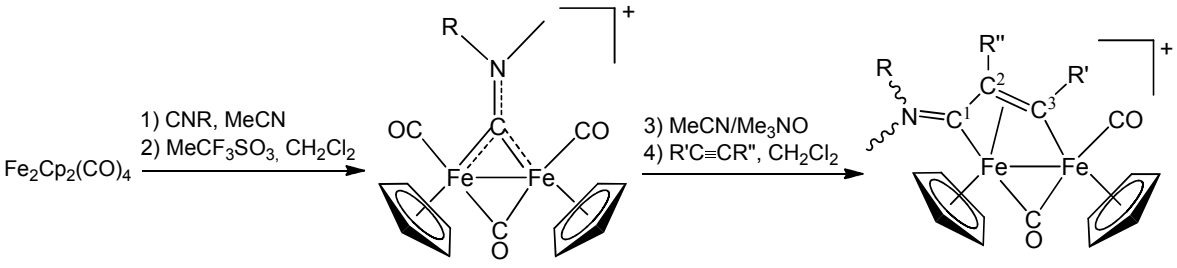

	R
[**1a**]$^+$	Me
[**1b**]$^+$	Xyl = 2,6-$C_6H_3Me_2$
[**1c**]$^+$	CH_2Ph

	R	*R′*	*R″*
[**2**]$^+$	Me	Ph	H
[**3**]$^+$	Me	2-naphthyl	H
[**4**]$^+$	Me	3-C_6H_4OH	H
[**5**]$^+$	Me	4-$C_6H_4CO_2H$	H
[**6**]$^+$	Me	3-thiophenyl	H
[**7**]$^+$	Me	Me	H
[**8**]$^+$	Me	CO_2Me	CO_2Me
[**9**]$^+$	Me	Me	Me
[**10**]$^+$	Me	Ph	Ph
[**11**]$^+$	Xyl	Ph	H
[**12**]$^+$	Xyl	Me	H
[**13**]$^+$	Xyl	CH_2OH	H
[**14**]$^+$	Xyl	3-thiophenyl	H
[**15**]$^+$	Xyl	2-naphthyl	H

[**16**]$^+$	Xyl	2-pyridyl	H
[**17**]$^+$	Xyl	CO_2Me	CO_2Me
[**18**]$^+$	Xyl	Me	Me
[**19**]$^+$	CH_2Ph	Ph	H

Scheme 1. Synthesis of diiron μ-vinyliminium complexes (with $CF_3SO_3^-$ as the counteranion).

Compounds [**7-13**]CF_3SO_3 and [**17-18**]CF_3SO_3 were reported previously,[27] whereas [**1-6**]CF_3SO_3, [**14-16**]CF_3SO_3 and [**19**]CF_3SO_3 are unprecedented. [**18**]CF_3SO_3 was primarily obtained in its *trans* form (with respect to the geometry of the Cp ligands),[30] before being quantitatively converted into the thermodynamically stable *cis* product upon gentle heating in methanol. The new products were characterized by IR, NMR (Figures S1-S37) and UV-Vis spectroscopy. The IR spectra, recorded in dichloromethane, display two intense absorptions related to the terminal and the bridging carbonyl ligands (e.g. at 1988 and 1809 cm^{-1} in [**3**]$^+$), as well as a band corresponding to the vibration of the [NC^1C^2] group in the range of 1662-1687 cm^{-1} ([**2-10**]$^+$ and [**19**]$^+$) and 1610-1632 cm^{-1} ([**11-18**]$^+$). The ^1H and ^{13}C NMR spectra of [**2-10**]CF_3SO_3 exhibit a single set of resonances, whereas E-Z isomerism due to the two possible orientations of the different N-substituents should in principle concern [**11-19**]CF_3SO_3. In [**19**]CF_3SO_3, containing N-substituents with comparable steric hindrance (i.e., methyl and benzyl), the E/Z ratio is ca. 3:2. Compounds [**11-18**]CF_3SO_3 comprise the encumbered xylyl group, and [**12**]CF_3SO_3 in particular exists exclusively in the E form; the same E orientation is prevalent in [**11**,**13-16**]CF_3SO_3 (E/Z ratio ranges from 4 to 9). Conversely [**17-18**]CF_3SO_3, bearing a C^2-substituent (R″), are found in the Z conformation, whereby the xylyl group points away from R″. The most salient NMR features are represented by the resonances of the C^1 and C^3 carbons, found between 218-233 ppm and 171-208 ppm, in agreement with their amino-alkylidene [31] and alkylidene nature,[32] respectively. The ^{19}F NMR spectra of [**2-19**]CF_3SO_3 (in D_2O) exhibit the singlet related to the triflate anion at ca. -79 ppm.

The X-ray structures of [**10**]CF_3SO_3, [**14**]$CF_3SO_3 \cdot 0.5CH_2Cl_2$, [**15**]$CF_3SO_3 \cdot CH_2Cl_2$ and [**16**]$CF_3SO_3 \cdot 0.5CH_2Cl_2$ were determined; a view of the cation [**10**]$^+$ is depicted in Figure 2, while the

other structures are shown in the Supporting Information together with a selection of geometric parameters (Figures S38-S40, Table S1). The organometallic cations are composed of a $[Fe_2Cp_2(CO)(\mu\text{-}CO)]$ skeleton, with the Cp-ligands in a *cis*-geometry, and a $[\mu\text{-}\eta^1\text{:}\eta^3\text{-}C^3(R')C^2HC^1N(Me)(Xyl)]^+$ vinyliminium ligand. The bridging alkylidene C^3 carbon is slightly asymmetric respect to the Fe centres, for instance in $[\mathbf{14}]^+$ Fe(2)-C(3) and Fe(1)-C(3) distances are 2.048(8) and 1.971(8) Å, respectively. The C(1)-N(1) distances are 1.284(3), 1.293(10), 1.313(12) and 1.294(12) Å in $[\mathbf{10}]^+$, $[\mathbf{14}]^+$, $[\mathbf{15}]^+$ and $[\mathbf{16}]^+$, respectively, in accordance with the iminium character; however, the Fe(2)-C(1) distances [1.842(2), 1.844(7), 1.832(11) and 1.852(3) Å in $[\mathbf{10}]^+$, $[\mathbf{14}]^+$, $[\mathbf{15}]^+$ and $[\mathbf{16}]^+$, respectively] are indicative of some aminoalkylidene nature.[31c,33] The iminium moiety displays an E-conformation that has been consistently detected by NMR spectroscopy (see above).

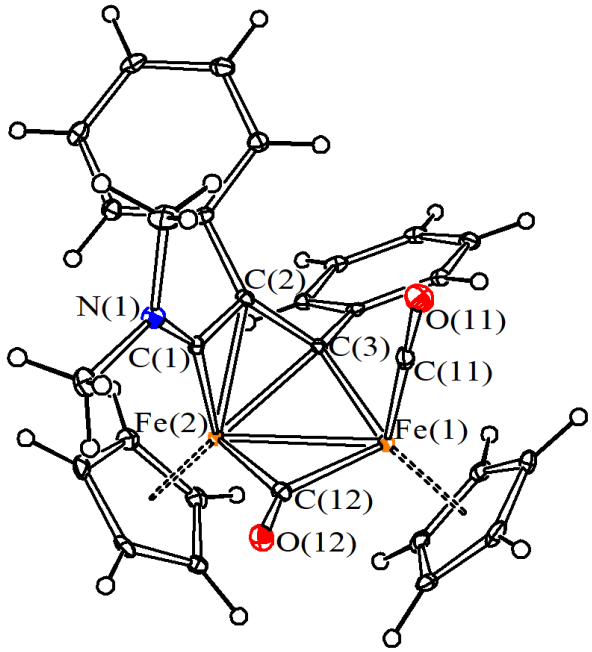

Figure 2. View of the structure of $[Fe_2Cp_2(CO)(\mu\text{-}CO)\{\mu\text{-}\eta^1\text{:}\eta^3\text{-}C^3(Ph)C^2(Ph)C^1NMe_2\}]^+$, $[\mathbf{10}]^+$. Displacement ellipsoids are at the 30% probability level.

2. Solubility and stability in aqueous media

Compounds [**2-19**]CF_3SO_3 possess amphiphilic character, being soluble in organic solvents such as dichloromethane and acetone as well as having appreciable solubility in water. The water solubility of [**2-19**]CF_3SO_3 was assessed at 21 °C in saturated D_2O solutions, monitored by ^1H NMR spectroscopy (Table 1).[34,35] The resulting solubility values fall within the range of $4.8 \cdot 10^{-4}$ – $9.8 \cdot 10^{-3}$ mol·L^{-1} (0.33 – 5.4 g·L^{-1}) and are comparable to some platinum-based drugs.[36,37] The presence of a Me substituent in place of a Xyl group on the iminium moiety generally leads to a two- to four-fold increase in water solubility (compare solubility ratios for Me/Xyl analogues [**2**]$^+$/[**11**]$^+$, [**3**]$^+$/[**15**]$^+$, [**6**]$^+$/[**14**]$^+$, [**8**]$^+$/[**17**]$^+$ and [**9**]$^+$/[**18**]$^+$), and [**4**]CF_3SO_3, [**7**]CF_3SO_3 and [**8**]CF_3SO_3 reach the highest values (~10^{-2} mol·L^{-1}). Interestingly, the *Z* isomers of [**11**,**14-16**] are prevalent in saturated D_2O solutions, whereas the E/Z ratio of these compounds in DMSO or acetone is >>1.

Octanol-water partition coefficients (Log P_{ow}, see Table 1) of [**2-19**]CF_3SO_3 were assessed spectrophotometrically using the shake-flask method (see Experimental for details).[34b] The majority of compounds displays an amphiphilic character (–0.5 < Log P_{ow} < 0.5), with the dimethyl-iminium derivatives [**2-10**]CF_3SO_3 being more hydrophilic than the N-Xyl complexes [**11-18**]CF_3SO_3.

Table 1. Solubility in D_2O (based on ^1H NMR spectroscopy, using Me_2SO_2 as an internal standard) and octanol-water partition coefficients (Log P_{ow}) of diiron complexes (all data refer to T = 21 °C).

Compound	Solubility in D_2O / mol·L^{-1}	Solubility in D_2O / g·L^{-1}	Log P_{ow}
[**2**]CF_3SO_3	$3.9 \cdot 10^{-3}$	2.4	–0.2
[**3**]CF_3SO_3	$1.8 \cdot 10^{-3}$	1.2	0.2
[**4**]CF_3SO_3	$1.4 \cdot 10^{-2}$	8.7	–0.34
[**5**]CF_3SO_3	$3.9 \cdot 10^{-3}$	2.5	–0.6
[**6**]CF_3SO_3	$3.5 \cdot 10^{-3}$	2.1	–0.12
[**7**]CF_3SO_3	$1.4 \cdot 10^{-2}$	7.6	–0.3
[**8**]CF_3SO_3	$1.9 \cdot 10^{-2}$	12	–1.0
[**9**]CF_3SO_3	$7.5 \cdot 10^{-3}$	4.2	–1.2
[**10**]CF_3SO_3	$4.3 \cdot 10^{-4}$	0.29	0.9
[**11**]CF_3SO_3	$9.4 \cdot 10^{-4}$	0.65	0.4
[**12**]CF_3SO_3	$1.0 \cdot 10^{-3}$	0.63	0.0

[**13**]CF_3SO_3	$1.0 \cdot 10^{-3}$	0.65	–0.1
[**14**]CF_3SO_3	$1.0 \cdot 10^{-3}$	0.70	0.5
[**15**]CF_3SO_3	$7.9 \cdot 10^{-4}$	0.59	1.4
[**16**]CF_3SO_3	$1.7 \cdot 10^{-3}$	1.2	0.1
[**17**]CF_3SO_3	$5.3 \cdot 10^{-3}$	3.9	–0.6
[**18**]CF_3SO_3	$2.0 \cdot 10^{-3}$	1.3	0.0
[**19**]CF_3SO_3	$4.6 \cdot 10^{-3}$	3.1	0.2

The stability of [**2-19**]CF_3SO_3 in D_2O or DMSO-d_6/D_2O solution was checked by ^1H NMR after 72 hours at 37 °C, these conditions resembling those of the cytotoxicity assays. A single set of signals was observed in the spectra of freshly-prepared solutions, attributed to the starting materials (two sets of signals in case of E/Z isomerism). No significant variation was observed by ^1H NMR after 72 hours, while a small amount of an orange-brown precipitate was noticed. In one case, the precipitate was isolated and identified as iron(III) oxide (haematite) by Raman analysis (see Experimental). It is presumable that slow, partial degradation in water liberates Fe^{2+} ions, then converted into Fe_2O_3. Substantial stability of [**2-19**]CF_3SO_3 was also observed in the presence of 0.1 M NaCl (D_2O or DMSO-d_6/D_2O solution).

The stability of [**2-19**]CF_3SO_3 in RPMI-1640 cell culture medium was monitored using IR spectroscopy and mass spectrometry and, with the exception of [**8**]CF_3SO_3 and [**17**]CF_3SO_3 which undergo extensive decomposition, the complexes showed good stability. It is possible that the observed degradation of [**8**]CF_3SO_3 and [**17**]CF_3SO_3 in cell culture medium is related to the presence of two CO_2Me substituents on the vinyliminium frame, that is known to favour nucleophilic additions to C[1].[38]

3. Spectro-electrochemical studies and reduction behaviour

The electrochemistry of selected complexes, i.e. [**7-9**]CF_3SO_3, [**11**]CF_3SO_3 and [**17-18**]CF_3SO_3, was investigated in both organic and aqueous solvents. In general, the investigated complexes showed CV profiles in THF/$[N^nBu_4]PF_6$ or CH_2Cl_2/$[N^nBu_4]PF_6$ involving a chemically reversible oxidation and two

reduction processes, complicated by subsequent chemical reactions (see Table 2 and Figures S41-S43). These findings are in accordance with the previous studies on $[Fe_2Cp_2(CO)(\mu\text{-}CO)\{\mu\text{-}\eta^1\text{:}\eta^3\text{-}C^3(Et)C^2HC^1N(Me)(Xyl)\}]CF_3SO_3$, [**20**]$CF_3SO_3$.[39]

Table 2. Formal electrode potential (V *vs.* $FeCp_2$) and peak-to-peak separations (mV) for redox processes in THF/$[N^nBu_4]PF_6$ 0.2 M.

	Reduction				***Oxidation***	
	E°'$_1$	**ΔE$_1$**[a]	**E°'$_2$**	**ΔE$_2$**[a]	**E°'$_3$**	**ΔE$_3$**[a]
[**7**]CF_3SO_3	==		−1.45	140	+0.55	90
[**8**]CF_3SO_3	−2.00[b]		−1.15	117	+0.88[b]	
[**9**]CF_3SO_3[d]	==		−1.49[b]		+0.62	95
[**11**]CF_3SO_3	−1.41	140	−1.30[b]		+0.66	110
[**17**]CF_3SO_3	−2.01[b]		−1.06	110	+0.97[b]	
[**18**]CF_3SO_3[d]	==		−1.41[c]	90	+0.70	90
[**20**]CF_3SO_3[39]	−1.48	95	−1.31	120	+0.62	92

[a] Measured at 0.1 V s^{-1}. [b] Peak potential value for irreversible processes. [c] Partially chemically reversible process. [d] In CH_2Cl_2/$[N^nBu_4]PF_6$ 0.2 M.

In a phosphate buffer solution (pH = 7.3), [**2**,**7**,**11**,**12**]CF_3SO_3 exhibit two chemically irreversible oxidations, falling in between +0.56 and +1.21 V (vs $FeCp_2$), whereas [**8**,**9**,**17**,**18**]CF_3SO_3 possess a single oxidation in the same range. These oxidations led to the deposition of degradation products on the surface of the carbon glassy working electrode. During the cathodic scan, one reduction peak was observed between –0.87 and –1.20 V (Table 3). In the reverse scan, an intense re-oxidation peak indicated accumulation of the electro-generated species on the electrode surface during the reduction step (Figure S44).

Table 3. Electrode potentials (V vs. $FeCp_2$ and in brackets vs. NHE) for redox processes of selected compounds in phosphate buffer solution at a carbon glassy electrode.

	Reduction [a]		Oxidation [a]	
Compound	E_{pc}	E_{pa} **(return peak)**	E_{pa1}	E_{pa2}
[**2**]CF_3SO_3	−1.12 (−0.71)	−0.40 (+0.01)	+0.61 (+1.02)	+0.86 (+1.27)
[**7**]CF_3SO_3	−1.14 (−0.73)	−0.49 (−0.08)	+0.71 (+1.12)	+1.02 (+1.43)
[**8**]CF_3SO_3	−0.99 (−0.58)	+0.10 (+0.51)	+0.87 (+1.28)	n.d.
[**9**]CF_3SO_3	−1.20 (−0.79)	−0.58 (−0.17)	+0.65 (+1.06)	n.d.
[**11**]CF_3SO_3	−0.98 (−0.57)	−0.56 (−0.15)	+0.56 (+0.97)	+0.97 (+1.38)
[**12**]CF_3SO_3	−0.92 (−0.51)	−0.46 (-0.05)	+0.71 (+1.12)	+1.21 (+1.62)
[**17**]CF_3SO_3	−0.87 (−0.46)	−0.26 (+0.15)	+1.04 (+1.45)	n.d.
[**18**]CF_3SO_3	−1.16 (−0.75)	−0.36 (+0.05)	+0.66 (+1.07)	n.d.

[a] Cathodic (E_{pc}) and anodic (E_{pa}) peak potentials measured at 0.1 V s^{-1}; n.d. = not detected.

The oxidation of [**2, 7-9, 11, 12, 7, 18**]CF_3SO_3 in phosphate buffer solution (pH = 7.3) occurs at potentials of E_{pa} > +0.95 V, which exceed those available in a biological environment where O_2 is the strongest oxidant (E° = +0.816 V vs NHE). The reduction potentials, however, range from -0.79 V for [**9**]CF_3SO_3 to -0.46 V for [**17**]CF_3SO_3, and the less negative values reach the biologically relevant range of potentials.[34b,40]

We recently demonstrated that the one-electron reduction of [**20**]CF_3SO_3 in THF solution triggers a cascade reaction leading to the formation of the iron(II) vinyl-aminoalkylidene complex **21a**, cyclopentadiene and atomic iron (Scheme 2). A similar response was observed for [**13**]CF_3SO_3, which converts into **21b** upon reaction with $CoCp_2$ (Scheme 2). Previously, compounds similar to **21a-b** (R =

Me or Xyl; R′ = alkyl or CO_2Me; R′ = H, alkyl or CO_2Me) were obtained by treatment of diiron vinyliminium precursors with sodium hydride[41] or, unexpectedly, tetrabutylammonium cyanide.[42]

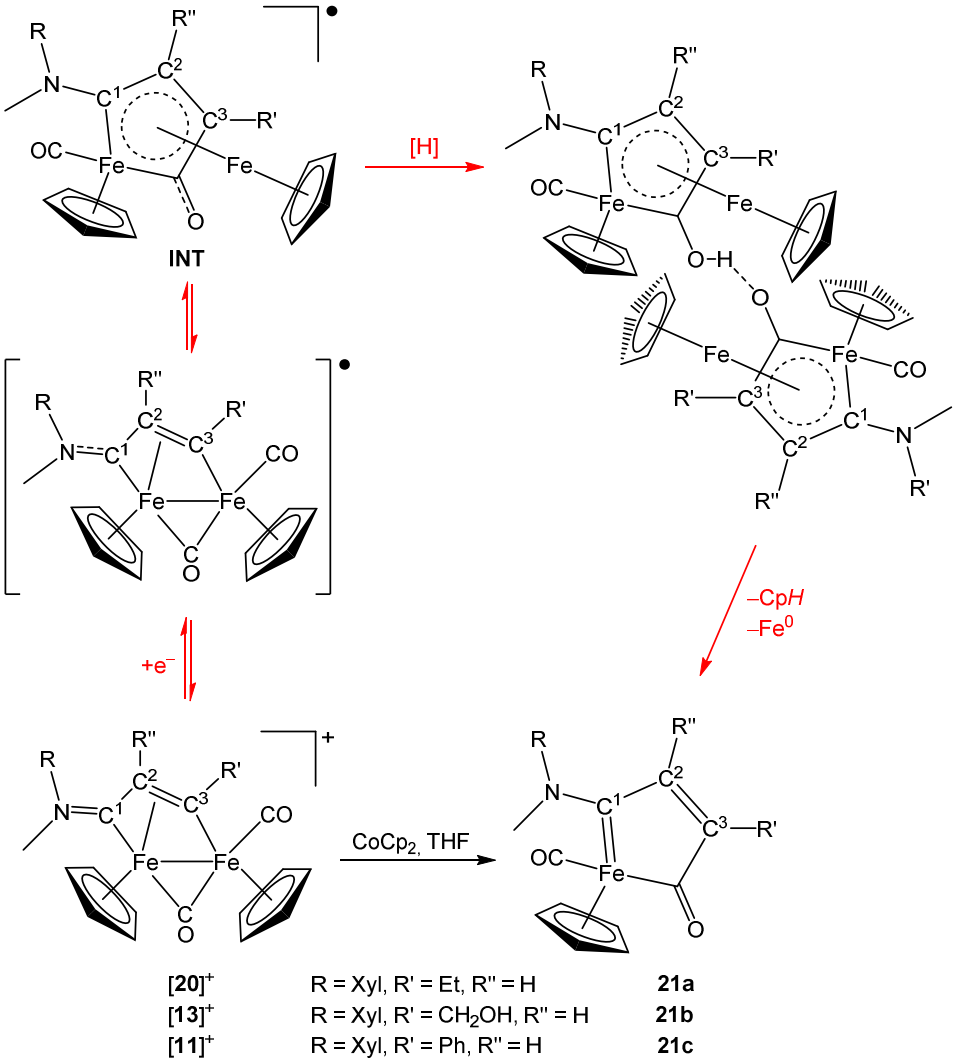

Scheme 2. Synthesis of Fe(II)-vinyl-aminoalkylidene complexes promoted by reduction of Fe(II)-Fe(II)-vinyliminium precursors, via Fe(0) elimination. Red pathway: mechanism proposed for the conversion of [**20**]$^+$ to **21a** on the basis of NMR, electrochemical, magnetometric and DFT studies.[39]

In order to determine whether the fragmentation reaction, leading to the production of **21a-b,** could be extended to compounds containing a R′ = aryl group, the reduction behaviour of [**11**]CF_3SO_3 was studied. The reaction of [**11**]CF_3SO_3 with $CoCp_2$ in anhydrous THF afforded [FeCp(CO){C^1N(Me)(Xyl)C^2HC^3(Ph)C(=O)}], **21c**, in high yield (Scheme 2). Compound **21c** was

fully characterized by analytical as well as spectroscopic methods, and its structure was confirmed by single crystal X-ray diffraction. The IR spectrum (in CH_2Cl_2) displays absorptions related to the carbonyl ligand, the acyl group and the aminocarbene-nitrogen bond at 1919, 1612 and 1571 cm^{-1}, respectively. The ^1H NMR spectrum (in acetone-d_6) consists of one set of resonances with the C^2H proton, occurring at 6.96 ppm, reflecting the alkenic nature of the $C^2=C^3$ interaction. The ^{13}C NMR spectrum shows the resonance of the C^1 carbon at 265 ppm which is in alignment with the aminoalkylidene character. The X-ray structure of **21c** (Figure 3) resembles that previously reported for **21a**, with the substituents around the partially double C^1-N bond arranged in the E configuration.[39]

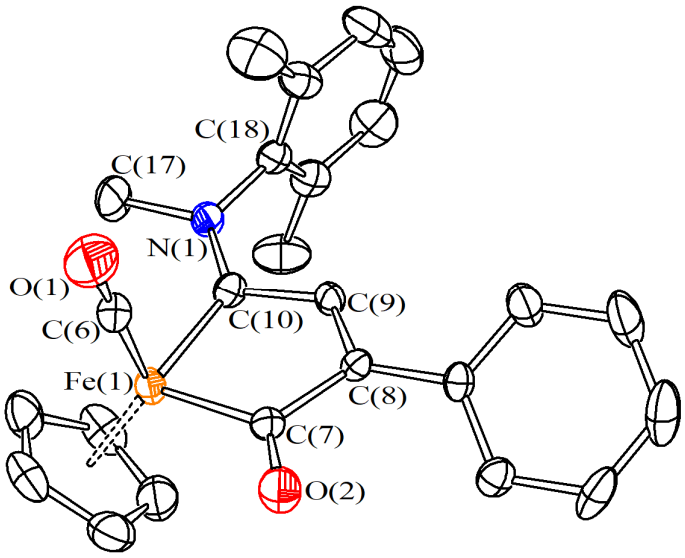

Figure 3. Molecular structure of [FeCp(CO){η^2-C^1Me(Xyl)C^2HC^3(Ph)C(=O)}], **21c**. Displacement ellipsoids are at the 30% probability level. H-atoms have been omitted for clarity. Selected bond lengths (Å) and angles (°): Fe(1)−C(7) 1.923(5), Fe(1)−C(10) 1.911(4), Fe(1)−C(6) 1.737(6), C(7)−C(8) 1.536(6), C(8)−C(9) 1.325(5), C(9)−−C(10) 1.459(5), C(10)−N(1) 1.325(5), C(6)−O(1) 1.129(5), C(7)−O(2) 1.211(5), C(7)−Fe(1)−C(10) 83.13(18), Fe(1)−C(7)−C(8) 113.5(3), C(7)−C(8)−C(9) 111.7(4), C(8)−C(9)−C(10) 116.3(4), C(9)−C(10)−Fe(1) 114.6(3), Fe(1)−C(6)−O(1) 178.3(5).

A spectro-electrochemical investigation on [**11**]CF_3SO_3 in THF/[N^nBu_4]PF_6 suggested that the formation of **21c** follows a pathway similar to the conversion of [**20**]$^+$ to **21a** (Scheme 2). Indeed, when the working electrode potential was slowly cycled between 0.0 and −1.7 V (scan rate 2 mV s^{-1}), the IR

absorptions of [**11**]$^+$ (1992, 1815, 1631, 1587 cm^{-1}) were initially replaced by new bands at 1951, 1594 and 1556 cm^{-1} (Figure S45A), corresponding to a ferra-ferrocene intermediate (**INT**, Scheme 2), where only one carbonyl ligand remains (Figure S45B). A residual, weak band at 1774 cm^{-1} might be due to traces of the unstable dinuclear radical species **11**. Bands at 1890, 1696, 1602 and 1591 cm^{-1} appeared at lower potentials, corresponding to [**INT**]$^-$. The bands of [**11**]$^+$ returned, together with a weak absorption at 1920 cm^{-1} related to **21c**, at the end of the return scan when the initial potential was reinstated (Figure S46).

Repeating the spectro-electrochemical study in a 0.2 M solution of H_2O in THF, no significant change was observed.[43] This outcome suggests that the production of **21c** from [**11**]CF_3SO_3 could be reproducible in an aqueous environment.

A cyclic voltammetry study on **21c** evidenced one accessible mono-electron oxidation ($E°' = -0.09$ V, ΔE_p = 66 mV) and one mono-electron reduction ($E°' = -1.87$ V, ΔE_p = 78 mV), both diffusion controlled and electrochemically and chemically reversible in the time scale of the experiment (Figure S47). In addition, in situ IR spectro-electrochemical analyses enabled the spectroscopic characterization of the oxidized and reduced products, [**21c**]$^+$ and [**21c**]$^-$ (Figure S48). The IR absorption of the carbonyl ligand was detected at 2025 cm^{-1} for [**21c**]$^+$ and at 1854 cm^{-1} for [**21c**]$^-$ (see Table S2 for details).

4. Cytotoxicity studies and assessment of ROS production

The cytotoxicity of [**2-19**]CF_3SO_3, **21b** and **21c** was assessed against cisplatin sensitive and cisplatin resistant human ovarian carcinoma (A2780 and A2780cisR) cell lines and the non-tumoural human embryonic kidney (HEK-293) cell line (Table 4). The cytotoxicity ranges from inactive (IC_{50} > 200 μM) to the nanomolar range. In general, the IC_{50} values of the diiron complexes correlate to the experimental Log P_{ow} values, i.e. with the cytotoxicity increasing with increasing lipophilicity.

Compounds [**11**]CF_3SO_3 (R = Xyl, R′ = Ph, R″ = H), [**15**]CF_3SO_3 (R = Xyl, R′ = 2-naphthyl, R″ = H) and [**18**]CF_3SO_3 (R = Xyl, R′ = Me, R″ = Me) are the most active against the A2780 cell line. On the other hand, [**5**]CF_3SO_3 (R = Me, R′ = 4-C_6H_4OH, R″ = H) and [**8**]CF_3SO_3 (R = Me, R′ = CO_2Me, R″ = CO_2Me) are inactive against all tested cell lines with IC_{50} values > 200 μM. Complexes [**3**,**10-16**,**18-19**]CF_3SO_3 all overcome cisplatin resistance in the A2780cisR cell line, with [**11**]CF_3SO_3 and [**15**]CF_3SO_3 possessing the lowest IC_{50} of 1.2 ± 0.2 μM compared to 26 ± 3 μM for cisplatin. A significant selectivity (S.I. values, Table 4) towards the A2780 cell line is observed compared to the non-tumoural HEK-293 cell line for [**1-2**,**7**,**10-11**,**16**,**18-19**]CF_3SO_3; in particular, [**10**]CF_3SO_3, presenting low micromolar cytotoxicity against the A2780 cells, exhibits nearly seven-fold selectivity. Interestingly, the benzyl compound [**19**]CF_3SO_3 afforded comparable IC_{50} values against A2780 and A2780cisR, and almost five-fold selectivity towards the cisplatin resistant cell line vs. the non tumoural cell line.

Complex **21c**, derived from $[\mathbf{11}]^+$, is cytotoxic against A2780 and A2780cisR cell lines, and has impressive selectivity (>12-fold) with respect to the HEK-293 cell line. On the other hand, **21b**, derived from $[\mathbf{13}]^+$, is essentially non cytotoxic.

Table 4. IC_{50} values (μM) determined for compounds [**2**-**19**]CF_3SO_3, **21b**, **21c** and cisplatin on human ovarian carcinoma (A2780), human ovarian carcinoma cisplatin resistant (A2780CisR) and human embryonic kidney (HEK-293) cell lines after 72 hours exposure. Values are given as the mean ± SD. Selectivity indexes (S.I.) calculated as ratio between IC_{50} values related to HEK-293 and A2780 cell lines.

Compound.	A2780	A2780cisR	HEK-293	S.I.
[**2**]CF_3SO_3	15 ± 2	72 ± 5	61 ± 4	4.1
[**3**]CF_3SO_3	2.9 ± 0.2	9.3 ± 0.7	12.0 ± 0.7	4.1
[**4**]CF_3SO_3	163 ± 16	172 ± 11	200 ± 21	1.2
[**5**]CF_3SO_3	> 200	> 200	> 200	==
[**6**]CF_3SO_3	30 ± 2	60 ± 4	33 ± 4	1.1
[**7**]CF_3SO_3	35 ± 3	86 ± 7	> 200	> 5.7

[**8**]CF_3SO_3	> 200	> 200	> 200	==
[**9**]CF_3SO_3	55 ± 3	107 ± 9	158 ± 12	2.9
[**10**]CF_3SO_3	1.8 ± 0.2	7.5 ± 0.3	12 ± 1	6.7
[**11**]CF_3SO_3	0.50 ± 0.06	1.2 ± 0.2	2.4 ± 0.2	4.8
[**12**]CF_3SO_3	2.7 ± 0.4	3.5 ± 0.6	2.2 ± 0.3	0.8
[**13**]CF_3SO_3	11.6 ± 0.6	21 ± 2	13.4 ± 1.0	1.2
[**14**]CF_3SO_3	2.1 ± 0.5	2.9 ± 0.3	2.2 ± 0.4	1.0
[**15**]CF_3SO_3	0.40 ± 0.06	1.2 ± 0.2	1.4 ± 0.1	3.5
[**16**]CF_3SO_3	1.4 ± 0.2	3.6 ± 0.1	5.8 ± 0.4	4.1
[**17**]CF_3SO_3	17.0 ± 0.8	35 ± 7	21.7 ± 1.4	1.3
[**18**]CF_3SO_3	0.90 ± 0.06	4.0 ± 0.3	5.0 ± 0.4	5.6
[**19**]CF_3SO_3	2.4 ± 0.3	2.8 ± 0.2	11.6 ± 0.4	4.8
21b	180 ± 1	> 200	> 200	==
21c	16 ± 2	26 ± 3	> 200	> 12
cisplatin	2.7 ± 0.1	26 ± 3	10.0 ± 0.7	3.7

Intracellular ROS production, induced by a selection of complexes, was monitored by fluorescence measurements using the DCFH-DA assay. A2780 and A2780cisR cells were continuously exposed to [**7**]CF_3SO_3, [**11**]CF_3SO_3, [**12**]CF_3SO_3, [**18**]CF_3SO_3, **21b**, **21c**, cisplatin (as a reference compound) and H_2O_2 (as a positive control). Appreciable intracellular ROS levels were observed after ca. 20 hours of treatment and progressively increased up to 24 hours (Figure 4). In particular, [**11**]CF_3SO_3 elicited a ROS production in A2780 cells close to that recorded for H_2O_2, whereas ROS formation triggered by exposure to **21b** and **21c** was considerably higher than the positive control (H_2O_2) in both A2780 and A2780cisR cell lines. The ROS level detected in the A2780 cell line treated with **21c** is significantly higher than that elicited by **21b**.

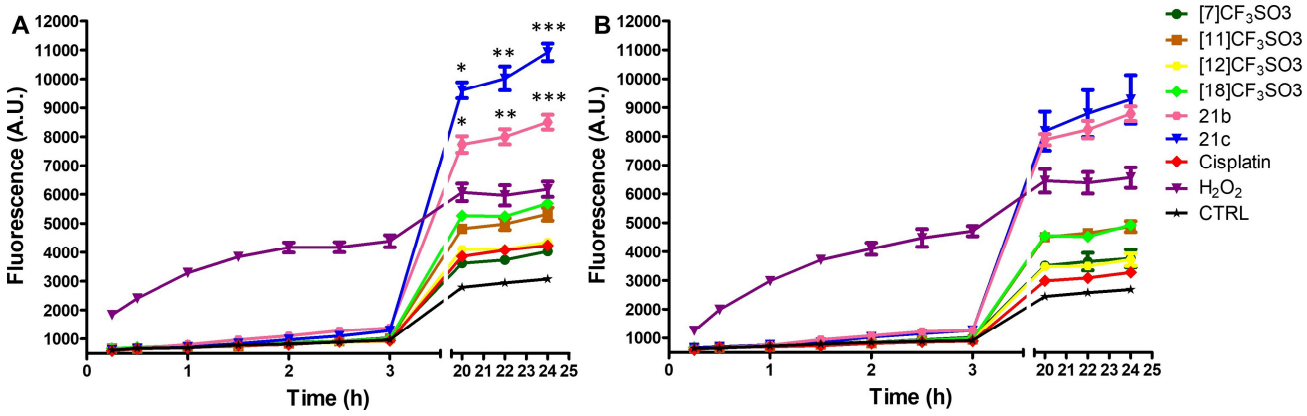

Figure 4. Fluorescence kinetics measurements of intracellular reactive oxygen species (ROS). (**A**) A2780 and (**B**) A2780cisR cells incubated for 24 hours with 100 μM of iron compounds at 37 °C. N.B.: values marked with the same number of * are significantly different when compared between each other ($p < 0.05$).

5. Interaction with biomolecules

The interaction of selected diiron complexes with a variety of biomolecules was studied to give insights into their mechanism of action. The reactivity of [**7**]CF_3SO_3 with a mononucleotide (guanosine 5'-monophosphate, 5'-GMP) and an oligonucleotide DNA model (14-mer, 5'-ATACATGGTACATA-3'), which have been used as models for other metallodrugs,[44] was evaluated. No significant interactions were observed between the mono- or oligonucleotide with [**7**]$^+$. Small shifts in the ^{1}H NMR spectrum (within 0.30 ppm) were detected after the incubation of [**7**]CF_3SO_3 with 5'-GMP compared to the spectra of the individual compounds. These shifts are influenced by the solution pH, most likely due to the different protonation states adopted by the phosphate group (pKa = 6.49 for PO_4^{2-} of 5'-GMP).[45]

The interaction of [**2**]CF_3SO_3, [**3**]CF_3SO_3, [**7**]CF_3SO_3, [**10**]CF_3SO_3, [**11**]CF_3SO_3, **21b** and **21c** with natural DNA was investigated using ethidium bromide displacement tests.[46] Calf-thymus DNA was saturated with ethidium bromide (EB), producing the known fluorescence emission increase at the wavelengths typical of the EB/DNA intercalated species (λ_{ex} = 520, λ_{em} = 595 nm). The addition of the selected diiron complexes resulted in a moderate drop in fluorescence indicating weak complex-DNA interactions through a non-intercalative binding mode (Figure 5). Interestingly, a significantly higher

DNA affinity was found for **21c**, probably favoured by the more hydrophobic and less sterically hindered structure respect to the cationic diiron frame. This increase of affinity is not displayed by the homologous compound **21b**, containing the alcohol function and lacking the phenyl group.

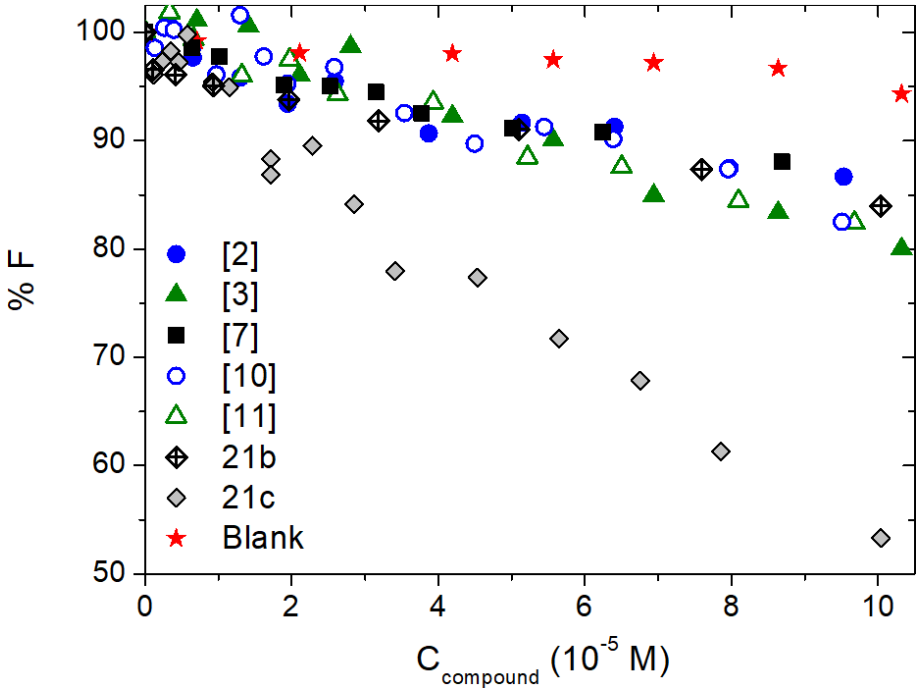

Figure 5. Ethidium bromide displacement tests for [**2**]CF_3SO_3, [**3**]CF_3SO_3, [**7**]CF_3SO_3, [**10**]CF_3SO_3, [**11**]CF_3SO_3, **21b** and **21c**: each complex was added to ethidium-saturated DNA; C_{DNA} = 1.4·10^{-4} M, C_{EB} = 5.9·10^{-5} M, NaCl 0.1 M, NaCac 0.01 M, λ_{ex} = 520 nm, λ_{em}= 595 nm, T = 25 °C.

The affinity of the diiron complexes to proteins was investigated using established peptide and protein models, i.e. amyloid β-protein (residues 1-16), ubiquitin and bovine serum albumin (BSA).[44,47] The interactions of [**7**]CF_3SO_3 with amyloid β-protein and ubiquitin were assessed using mass spectrometry. Following incubation, no adducts were found but [**7**]$^+$ was observed as an unbound cation (*m/z* 394.019) alongside additional peaks related to the loss of one (*m/z* 366.023) and two (*m/z* 338.029) carbonyls. The overall positively charged biomolecules were identified in association with one, two or three triflate anions. Mass spectrometry analyses of BSA incubated with [**2**]CF_3SO_3, [**7**]CF_3SO_3, [**10**]CF_3SO_3 and [**11**]CF_3SO_3 led to recognition of the respective complex cation peaks, but

no adduct identification. Additionally, the interaction of [**2**]CF_3SO_3, [**7**]CF_3SO_3, [**10**]CF_3SO_3 and [**11**]CF_3SO_3 with BSA was assessed using direct spectrofluorimetric titrations where aliquots of the complex were added to a BSA solution (λ_{ex} = 280 nm, λ_{em} = 345 nm). For all tested complexes, a decrease in BSA fluorescence emissions was observed (Figure S49). A Stern-Volmer analysis of the fluorescence data at different temperatures (10-40 °C range, Table S3) agrees with the static quenching of the protein emission suggesting adduct formation.[48] Equilibrium data for the distinct systems at variable temperatures were evaluated using the HypSpec® software and reported in the form of a van't Hoff plot (Supporting Information, Figures S50-S51). Due to the narrow temperature range and the application of a simple model to the complex protein substrate, the trends must be considered as indicative. [**2**]CF_3SO_3, [**7**]CF_3SO_3, [**10**]CF_3SO_3 and [**11**]CF_3SO_3 lie in a common stripe and display positive ΔH and ΔS values. This data outlines entropically driven hydrophobic interactions,[49] suggesting that the protein binding does not significantly contribute to the anticancer activity.

6. Final remarks on the cytotoxic activity

The diiron complexes probably exert their cytotoxicity by means of more than one mechanism of action, involving ROS production and limited interactions with DNA, but not proteins. Clean fragmentation, initiated by mono-electron reduction, might be viable for those compounds containing R and/or R′ electron withdrawing groups, according to electrochemical data. This reaction is expected to proceed via Fe(0) elimination leading to mononuclear Fe(II) derivatives (Scheme 2), with different antiproliferative activities (compare data on **21b** and **21c**). It is possible that the high level of cytotoxicity and the significant selectivity detected for [**11**]CF_3SO_3 is correlated to its partial conversion into **21c**, which exhibits a cytotoxic behaviour ascribable to both ROS generation (allowed by accessible oxidation potential) and DNA binding.

Conclusions

Cationic diiron vinyliminium complexes, in the form of their triflate salts, possess an amphiphilic nature due to the combination of net positive charge with non-polar fragments. They exhibit acceptable water solubility and are reasonably stable in water and cell culture medium. Their structure and physico-chemical properties can be modulated by adjusting the isocyanide/alkyne combination that generates the vinyliminium moiety. The availability of commercial alkynes, the large scope and the regio-specificity of the alkyne insertion reaction, tolerating various functional groups (Scheme 1), offers wide structural variability. We synthesized a series of vinyliminium complexes, including novel complexes containing various functionalities within the vinyliminium frame, which was assessed for the antiproliferative activity. In general, the activity is variable, ranging from inactive to nanomolar concentrations, against A2780 and A2780cisR cell lines. A general trend indicates that the IC_{50} values decrease with increasing lipophilicity but, importantly, the complexes remain water soluble. Up to a seven fold selectivity has been observed towards the cancerous A2780 cell line compared to the non-tumoural HEK-293 cell line for the most active complexes. Investigations suggest that multiple effects could be responsible for the cytotoxicity of the complexes, including ROS production and DNA binding, but not protein binding. The ROS generation and especially the DNA binding may be enhanced by fragmentation of the diiron compounds to monoiron species.

Experimental

1. Synthetic procedures and characterization of products

General details. Organic reactants (TCI Europe or Merck) and $Fe_2Cp_2(CO)_4$ (Strem) were commercial products of the highest purity available. Compounds [**1a-c**]CF_3SO_3 [27] and [**10**]CF_3SO_3 [50] were prepared according to published procedures. Chromatography separations were carried out on columns of deactivated alumina (Merck, 4% *w/w* water). Infrared spectra of solid samples were recorded on a Perkin Elmer Spectrum One FT-IR spectrometer, equipped with a UATR sampling accessory (4000-400 cm^{-1} range). Infrared spectra of solutions were recorded on a Perkin Elmer Spectrum 100 FT-IR spectrometer with a CaF_2 liquid transmission cell (2300-1500 cm^{-1} range). UV-Vis spectra were recorded on an Ultraspec 2100 Pro spectrophotometer. IR and UV-Vis spectra were processed with Spectragryph software.[51] NMR spectra were recorded at 298 K on a Bruker Avance II DRX400 instrument equipped with a BBFO broadband probe. Chemical shifts (expressed in parts per million) are referenced to the residual solvent peaks [52] (^1H, ^{13}C) or to external standard (^{19}F, $CFCl_3$). NMR spectra were assigned with the assistance of ^1H-^{13}C (*gs*-HSQC and *gs*-HMBC) correlation experiments.[53] NMR signals due to a second isomeric form are italicized. RAMAN analysis was conducted with a Renishaw Invia micro-Raman instrument equipped with a Nd:YAG laser working at 532 nm and 0.1 mW, integration time 10 s. Carbon, hydrogen and nitrogen analyses were performed on a Vario MICRO cube instrument (Elementar).

Synthesis of diiron vinyliminium complexes. In a typical procedure, [**1a-c**]CF_3SO_3 (ca. 0.5 mmol) was dissolved into acetonitrile (10 mL) and treated with Me_3NO (1.3 eq.). The resulting mixture was stirred for 1 hour, and progressive darkening of the solution was observed. The complete conversion of the starting material into the acetonitrile adduct $[Fe_2Cp_2(CO)(\mu\text{-}CO)(NCMe)\{\mu\text{-}CNMe(R)\}]CF_3SO_3$ (R = Me, Xyl, CH_2Ph) was confirmed by IR spectroscopy. The volatiles were removed under vacuum, thus

the dark brown residue was dissolved into dichloromethane (ca. 20 mL). The solution was treated with the appropriate alkyne (ca. 1.3 eq.), and the mixture was stirred at room temperature for 48 hours, under a nitrogen atmosphere. The final mixture was charged on an alumina column. Elution with CH_2Cl_2 and CH_2Cl_2/THF mixtures allowed the removal of unreacted alkyne and impurities, then a fraction corresponding to the desired product was collected using MeCN/MeOH 9:1 (v/v) as eluent. Removal of the solvent under reduced pressure afforded the product. Compounds [**2**,**7-9**,**11-12**,**17-18**]CF_3SO_3 were prepared in comparable yields also in gram-scale quantities (1-4 g), without any modification of the general procedure. All compounds, [**1-19**]CF_3SO_3, resulted indefinitely air stable.

[$Fe_2Cp_2(CO)(\mu\text{-}CO)\{\mu\text{-}\eta^1\text{:}\eta^3\text{-}C^3(Ph)C^2HC^1NMe_2\}$]$CF_3SO_3$, [2]$CF_3SO_3$ (Chart 1)

Chart 1. Structure of [**2**]$^+$.

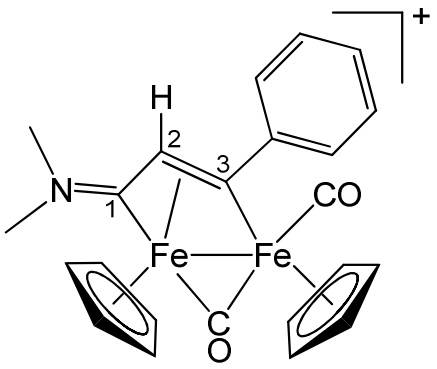

From [**1a**]CF_3SO_3 and phenylacetylene. Brown solid, yield 74%. Anal. calcd. for $C_{24}H_{22}F_3Fe_2NO_5S$: C, 47.63; H, 3.66; N, 2.31. Found: C, 47.39; H, 3.80; N, 2.45. IR (CH_2Cl_2): $\tilde{\upsilon}$/cm^{-1} = 1993vs (CO), 1809s (μ-CO), 1677m (C^2C^1N). ^{1}H NMR (acetone-d_6): δ/ppm = 7.84, 7.57, 7.43 (m, 5 H, Ph); 5.44, 5.25 (s, 10 H, Cp); 4.68 (s, 1 H, C^2H); 4.05, 3.47 (s, 6 H, NMe). $^{13}C\{^1H\}$ NMR (acetone-d_6): δ/ppm = 255.9 (μ-CO); 225.0 (C^1); 210.1 (CO); 203.8 (C^3); 156.3 (*ipso*-Ph); 128.4, 127.5, 127.0 (Ph); 91.6, 87.8 (Cp); 53.0 (C^2); 51.1, 44.4 (NMe). ^{1}H NMR (D_2O): δ/ppm = 7.67, 7.51, 7.38 (m, 5 H, Ph); 5.16, 5.04 (s, 10

H, Cp); 4.49 (s, 1 H, C^2H); 3.79, 3.23 (s, 6 H, NMe). ^{19}F NMR (D_2O): δ/ppm = –78.9. λ_{max}/nm ($\varepsilon/M^{-1}\cdot cm^{-1}$, CH_2Cl_2) = 223 ($4.8\cdot10^4$), 270 ($2.4\cdot10^4$).

$[Fe_2Cp_2(CO)(\mu\text{-}CO)\{\mu\text{-}\eta^1\text{:}\eta^3\text{-}C^3(2\text{-naphthyl})C^2HC^1NMe_2\}]CF_3SO_3$, $[\mathbf{3}]CF_3SO_3$ (Chart 2)

Chart 2. Structure of $[\mathbf{3}]^+$.

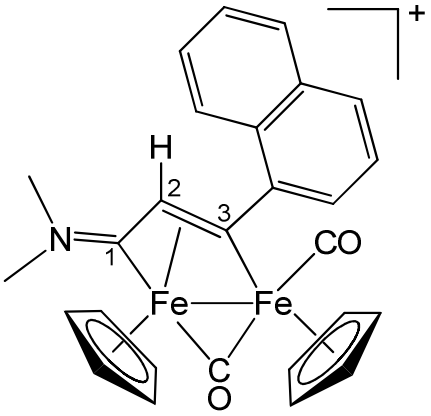

From [**1a**]CF_3SO_3 and 1-ethynylnaphthalene. Brown solid, yield 96%. Anal. calcd. for $C_{28}H_{24}F_3Fe_2NO_5S$: C, 51.32; H, 3.69; N, 2.14. Found: C, 51.24; H, 3.73; N, 2.24. IR (CH_2Cl_2): $\tilde{\upsilon}/cm^{-1}$ = 1988vs (CO), 1809s (μ-CO), 1687m (C^2C^1N). ^1H NMR (dmso-d_6): δ/ppm = 8.08, 8.01, 7.88, 7.74, 7.60 (m, 7 H, $C_{10}H_7$); 5.48, 5.06 (s, 10 H, Cp); 4.73 (s, 1 H, C^2H); 3.90, 3.33 (s, 6 H, NMe). $^{13}C\{^1H\}$ NMR (dmso-d_6): δ/ppm = 257.0 (*μ*-CO); 224.1 (C^1); 211.5 (CO); 202.7 (C^3); 153.0 (*ipso*-$C_{10}H_7$); 133.8, 129.9, 129.0, 127.6, 127.1, 126.5, 126.3, 125.7 ($C_{10}H_7$); 92.3, 88.5 (Cp); 54.8 (C^2); 51.8, 44.7 (NMe). ^1H NMR (D_2O): δ/ppm = 7.98, 7.70, 7.57 (m, 7 H, $C_{10}H_7$); 5.28, 4.90 (s, 10 H, Cp); 4.63 (s, 1 H, C^2H); 3.84, 3.30 (s, 6 H, NMe). ^{19}F NMR (D_2O): δ/ppm = –78.9. λ_{max}/nm ($\varepsilon/M^{-1}\cdot cm^{-1}$, CH_2Cl_2) = 228 ($4.9\cdot10^4$), 310 ($1.5\cdot10^4$).

$[Fe_2Cp_2(CO)(\mu\text{-}CO)\{\mu\text{-}\eta^1\text{:}\eta^3\text{-}C^3(3\text{-}C_6H_4OH)C^2HC^1NMe_2\}]CF_3SO_3$, $[\mathbf{4}]CF_3SO_3$ (Chart 3)

Chart 3. Structure of $[\mathbf{4}]^+$.

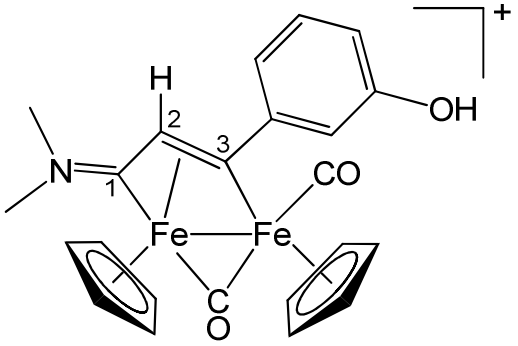

From [**1a**]CF_3SO_3 and 3-hydroxyphenylacetylene. Brown solid, yield 71%. Anal. calcd. for $C_{24}H_{22}F_3Fe_2NO_6S$: C, 46.40; H, 3.57; N, 2.25. Found: C, 46.30; H, 3.49; N, 2.36. IR (CH_2Cl_2): ϋ/cm^{-1} = 1990vs (CO), 1806s (μ-CO), 1675m (C^2C^1N), 1593 (arom). ^{1}H NMR (acetone-d_6): δ/ppm = 8.87 (br, 1 H, OH); 7.36, 7.22, 6.88 (m, 4 H, C_6H_4); 5.39, 5.25 (s, 10 H, Cp); 4.63 (s, 1 H, C^2H); 4.02, 3.44 (s, 6 H, NMe). $^{13}C\{^1H\}$ NMR (acetone-d_6): δ/ppm = 256.1 (*μ*-CO); 225.1 (C^1); 211.1 (CO); 204.1 (C^3); 157.6, 157.4 (*ipso*-C_6H_4 + COH); 129.4, 118.5, 114.3, 114.0 (C_6H_4); 91.7, 87.7 (Cp); 52.6 (C^2); 50.8, 44.2 (NMe). ^{1}H NMR (D_2O): δ/ppm = 7.38, 7.22, 7.13, 6.88 (m, 4 H, C_6H_4OH); 5.15, 5.04 (s, 10 H, Cp); 4.48 (s, 1 H, C^2H); 3.78, 3.22 (s, 6 H, NMe). ^{19}F NMR (D_2O): δ/ppm = –78.9. λ_{max}/nm (ε/$M^{-1}\cdot cm^{-1}$, CH_2Cl_2) = 224 ($4.2\cdot10^4$), 269 ($1.8\cdot10^4$), 300 ($1.5\cdot10^4$).

[Fe_2Cp_2(CO)(μ-CO){μ-η^1:η^3-C^3(4-$C_6H_4CO_2H$)$C^2HC^1NMe_2$}]CF_3SO_3, [5]CF_3SO_3 (Chart 4)

Chart 4. Structure of [**5**]$^+$.

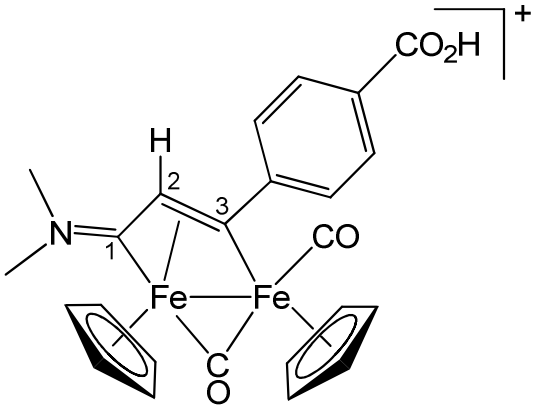

From [**1a**]CF_3SO_3 and 4-ethynylbenzoic acid. Brown-green solid, yield 87%. Anal. calcd. for $C_{25}H_{22}F_3Fe_2NO_7S$: C, 46.25; H, 3.42; N, 2.16. Found: C, 46.07; H, 3.53; N, 2.25. IR (CH_2Cl_2): ϋ/cm^{-1} = 1993vs (CO), 1807s (μ-CO), 1697m (COOH), 1677m (C^2C^1N), 1604w (C=C), 1590w (C=C). ^1H NMR (acetone-d_6): δ/ppm = 8.19, 7.96 (br, 4 H, C_6H_4); 5.46, 5.27 (s, 10 H, Cp); 4.73 (s, 1 H, C^2H); 4.05, 3.48 (s, 6 H, NMe). $^{13}C\{^1H\}$ NMR (acetone-d_6): δ/ppm = 255.3 (μ-CO); 224.6 (C^1); 209.8 (CO); 201.0 (C^3); 166.5 (CO_2H); 160.5, 150.0 (*ipso*-C_6H_4); 129.8, 127.7 (*orto*-C_6H_4 + *meta*-C_6H_4); 91.6, 87.8 (Cp); 52.7 (C^2); 51.0, 44.2 (NMe). ^1H NMR (D_2O): δ/ppm = 7.98, 7.70 (m, 4 H, C_6H_4); 5.18, 5.04 (s, 10 H, Cp); 4.54 (s, 1 H, C^2H); 3.79, 3.23 (s, 6 H, NMe). ^{19}F NMR (D_2O): δ/ppm = –78.6. λ_{max}/nm (ε/$M^{-1}\cdot cm^{-1}$, CH_2Cl_2) = 223 ($3.1\cdot10^4$), 268 ($1.8\cdot10^4$).

[Fe_2Cp_2(CO)(μ-CO){μ-η^1:η^3-C^3(3-tiophenyl)$C^2HC^1NMe_2$}]CF_3SO_3, [6]CF_3SO_3 (Chart 5)

Chart 5. Structure of [**6**]$^+$.

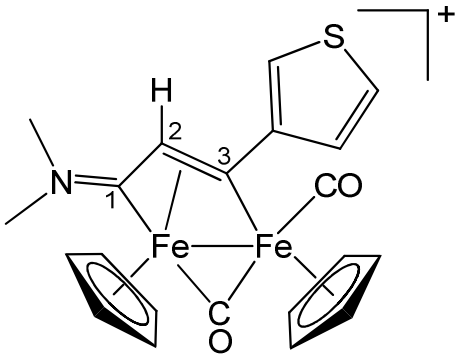

From [**1a**]CF_3SO_3 and 3-ethynylthiophene. Brown solid, yield 71%. Anal. calcd. for $C_{22}H_{20}F_3Fe_2NO_5S_2$: C, 43.23; H, 3.30; N, 2.29. Found: C, 43.11; H, 3.37; N, 2.40. IR (CH_2Cl_2): ϋ/cm^{-1} = 1991vs (CO), 1808s (μ-CO), 1687m (C^2C^1N), 1606w-m (arom). ^1H NMR (acetone-d_6): δ/ppm = 7.82, 7.72 (m, 3 H, C_4H_3S); 5.36, 5.33 (s, 10 H, Cp); 4.72 (s, 1 H, C^2H); 4.04, 3.45 (s, 6 H, NMe). $^{13}C\{^1H\}$ NMR (acetone-d_6): δ/ppm = 255.9 (μ-CO); 225.2 (C^1); 210.1 (CO); 195.4 (C^3); 157.6 (*ipso*-C_4H_3S); 129.3, 126.2, 120.1 (C_4H_3S); 91.4, 87.8 (Cp); 52.5 (C^2); 50.9, 44.2 (NMe). ^1H NMR (D_2O):

δ/ppm = 7.56, 7.51 (m, 3 H, C_4H_3S); 5.10, 5.09 (s, 10 H, Cp); 4.53 (s, 1 H, C^2H); 3.76, 3.21 (s, 6 H, NMe_2). ^{19}F NMR (D_2O): δ/ppm = –78.9. λ_{max}/nm (ε/$M^{-1}\cdot cm^{-1}$, CH_2Cl_2) = 223 ($5.2\cdot10^4$), 264 ($2.6\cdot10^4$), 302 ($2.0\cdot10^4$).

$[Fe_2Cp_2(CO)(\mu\text{-}CO)\{\mu\text{-}\eta^1\text{:}\eta^3\text{-}C^3(Me)C^2HC^1NMe_2\}]CF_3SO_3$, $[7]CF_3SO_3$ (Chart 6)

Chart 6. Structure of $[7]^+$.

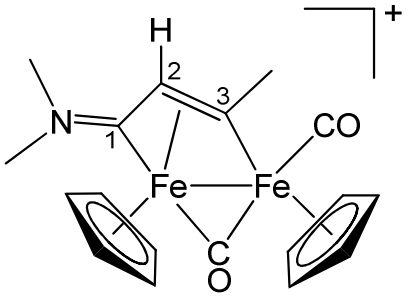

From [**1a**]CF_3SO_3 and propyne (in THF solution, ca. 1 mol/L). Brown solid, yield 96%. Anal. calcd. for $C_{19}H_{20}F_3Fe_2NO_5S$: C, 42.02; H, 3.71; N, 2.58. Found: C, 41.89; H, 3.64; N, 2.68. IR (CH_2Cl_2): ῡ/cm^{-1} = 1990vs (CO), 1806s (μ-CO), 1684m (C^2C^1N). ^1H NMR (dmso-d_6): δ/ppm = 5.48, 5.14 (s, 10 H, Cp); 4.51 (s, 1 H, C^2H); 3.82, 3.77 (s, 6 H, NMe + C^3Me); 3.18 (s, 6 H, NMe). $^{13}C\{^1H\}$ NMR (dmso-d_6): δ/ppm = 258.4 (μ-CO); 225.6 (C^1); 211.4 (CO); 208.0 (C^3); 91.2, 88.0 (Cp); 52.1 (C^2); 51.0, 44.8 (NMe_2); 41.7 (C^3Me). ^1H NMR (D_2O): δ/ppm = 5.28, 4.94 (s, 10 H, Cp); 4.39 (s, 1 H, C^2H); 3.75, 3.70 (s, 6 H, NMe + C^3Me); 3.13 (s, 3 H, NMe). ^{19}F NMR (D_2O): δ/ppm = –78.9. λ_{max}/nm (ε/$M^{-1}\cdot cm^{-1}$, CH_2Cl_2) = 226 ($2.4\cdot10^4$), 294 ($8.6\cdot10^3$), 406 ($2.5\cdot10^3$).

$[Fe_2Cp_2(CO)(\mu\text{-}CO)\{\mu\text{-}\eta^1\text{:}\eta^3\text{-}C^3(CO_2Me)C^2(CO_2Me)C^1NMe_2\}]CF_3SO_3$, $[8]CF_3SO_3$ (Chart 7)

Chart 7. Structure of $[8]^+$.

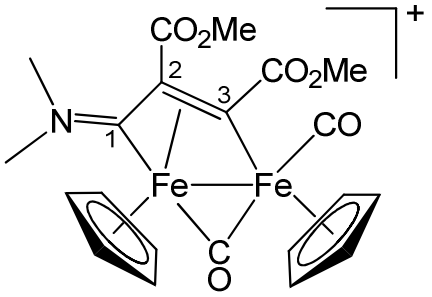

From [**1a**]CF_3SO_3 and dimethyl acetylenedicarboxylate. Brown solid, yield 88%. Anal. calcd. for $C_{22}H_{23}F_3Fe_2NO_9S$: C, 40.89; H, 3.59; N, 2.17. Found: C, 40.95; H, 3.38; N, 2.25. IR (CH_2Cl_2): $\tilde{\upsilon}/cm^{-1}$ = 2007vs (CO), 1830s (μ-CO), 1733s (CO_2Me), 1715s (CO_2Me), 1685m (C^2C^1N). ^1H NMR (dmso-d_6/D_2O 3:1): δ/ppm = 5.37, 5.22 (s, 10 H, Cp); 4.01, 3.83 (s, 6 H, CO_2Me); 3.74, 3.19 (s, 6 H, NMe_2). $^{13}C\{^1H\}$ NMR (dmso-d_6/D_2O 3:1): δ/ppm = 251.6 (*μ*-CO); 218.2 (C^1); 208.7 (CO); 187.3 (C^3); 176.8, 166.8 (*C*O_2Me); 92.1, 89.9 (Cp); 52.5 (C^2); 54.1, 53.3 (CO_2*Me*); 51.8, 45.6 (NMe). ^1H NMR (D_2O): δ/ppm = 5.30, 5.15 (s, 10 H, Cp); 4.09, 3.83 (s, 6 H, CO_2Me); 3.78, 3.22 (s, 6 H, NMe_2). ^{19}F NMR (D_2O): δ/ppm = –78.9. λ_{max}/nm ($\varepsilon/M^{-1}\cdot cm^{-1}$, CH_2Cl_2) = 226 ($3.2\cdot10^4$), 291 ($1.4\cdot10^4$), 389 ($4.3\cdot10^3$).

$[Fe_2Cp_2(CO)(\mu\text{-}CO)\{\mu\text{-}\eta^1\text{:}\eta^3\text{-}C^3(Me)C^2(Me)C^1NMe_2\}]CF_3SO_3$, [9]$CF_3SO_3$ (Chart 8)

Chart 8. Structure of $[\mathbf{9}]^+$.

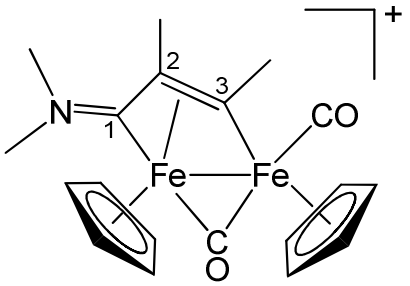

From [**1a**]CF_3SO_3 and 2-butyne. Dark green solid, yield 94%. Anal. calcd. for $C_{20}H_{22}F_3Fe_2NO_5S$: C, 43.12; H, 3.98; N, 2.51. Found: C, 42.90; H, 3.91; N, 2.60. IR (CH_2Cl_2): $\tilde{\upsilon}/cm^{-1}$ = 1987vs (CO), 1806s (μ-CO), 1665m (C^2C^1N). ^1H NMR (dmso-d_6): δ/ppm = 5.44, 5.11 (s, 10 H, Cp); 3.74 (s, 3 H, C^3Me);

3.70, 3.09 (s, 6 H, NMe_2); 1.83 (s, 3 H, C^2Me). ^1H NMR (D_2O): δ/ppm = 5.23, 4.89 (s, 10 H, Cp); 3.67, 3.65 (s, 6 H, C^3Me + NMe); 2.61 (s, 3 H, NMe); 1.76 (s, 3 H, C^2Me). ^{19}F NMR (D_2O): δ/ppm = –78.8. λ_{max}/nm (ε/$M^{-1}\cdot cm^{-1}$, CH_2Cl_2) = 225 ($3.2\cdot10^4$), 265 ($1.2\cdot10^4$), 295 ($1.1\cdot10^4$).

$[Fe_2Cp_2(CO)(\mu\text{-}CO)\{\mu\text{-}\eta^1\text{:}\eta^3\text{-}C^3(Ph)C^2(Ph)C^1NMe_2\}]CF_3SO_3$, $[\mathbf{10}]CF_3SO_3$ (Chart 9)

Chart 9. Structure of $[\mathbf{10}]^+$.

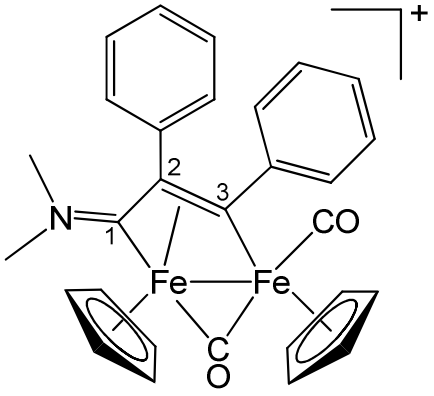

From $[\mathbf{1a}]CF_3SO_3$ and diphenylacetylene. Dark green solid, yield 52%. Crystals suitable to X-ray analysis were obtained from a concentrated water/dmso solution at 20 °C. Anal. calcd. for $C_{30}H_{26}F_3Fe_2NO_5S$: C, 52.89; H, 3.85; N, 2.06. Found: C, 52.80; H, 3.72; N, 2.13. IR (CH_2Cl_2): ῡ/cm^{-1} = 1995vs (CO), 1813s (μ-CO), 1662m (C^2C^1N). ^1H NMR (acetone-d_6): δ/ppm = 7.86, 7.58, 7.41, 7.28, 7.20, 7.14 (m, 10 H, Ph); 5.67, 5.29 (s, 10 H, Cp); 4.11, 2.85 (s, 6 H, NMe). ^1H NMR (D_2O): δ/ppm = 7.20, 7.12, 7.01 (m, 7 H, $C_{10}H_7$); 5.40, 5.06 (s, 10 H, Cp); 3.82, 2.88 (s, 6 H, NMe_2). λ_{max}/nm (ε/$M^{-1}\cdot cm^{-1}$, CH_2Cl_2) = 241 ($4\cdot10^4$), 323 ($5\cdot10^3$).

$[Fe_2Cp_2(CO)(\mu\text{-}CO)\{\mu\text{-}\eta^1\text{:}\eta^3\text{-}C^3(Ph)C^2HC^1N(Me)(Xyl)\}]CF_3SO_3$, $[\mathbf{11}]CF_3SO_3$ (Chart 10)

Chart 10. Structure of $[\mathbf{11}]^+$.

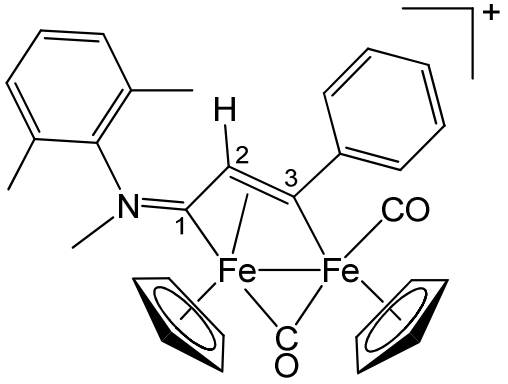

From [**1b**]CF_3SO_3 and phenylacetylene. Brown, yield 74%. Anal. calcd. for $C_{31}H_{28}F_3Fe_2NO_5S$: C, 53.55; H, 4.06; N, 2.01. Found: C, 53.68; H, 3.93; N, 2.07. IR (CH_2Cl_2): $\tilde{\upsilon}$/cm^{-1} = 2003vs (CO), 1819s (μ-CO), 1629m (C^2C^1N). ^{1}H NMR (dmso-d_6/D_2O 3:1): δ/ppm = 7.46, 7.38, 7.23, 7.06 (8 H, Ph + $C_6H_3Me_2$); 5.61, 5.33, *5.28*, *4.97* (s, 10 H, Cp); 4.25, *3.58* (s, 3 H, NMe); 4.10 (s, 1 H, C^-H); 2.22, 1.78 (s, 6 H, $C_6H_3Me_2$), E/Z ratio = 9. ^{1}H NMR (D_2O): δ/ppm = *5.38*, *5.16*, 5.11, 4.88 (s, 10 H, Cp); *4.18*, 3.53 (s, 3 H, NMe); 2.41, *2.12*, 1.94, *1.82* (s, 6 H, $C_6H_3Me_2$), Z/E ratio = ca. 1.5. λ_{max}/nm (ε/M^{-1}·cm^{-1}, CH_2Cl_2) = 227 ($3.0\cdot10^4$), 269 ($1.5\cdot10^4$), 304 ($1.1\cdot10^4$).

[Fe_2Cp_2(CO)(μ-CO){μ-η^1:η^3-C^3(Me)C^2HC^1N(Me)(Xyl)}]CF_3SO_3, [12]CF_3SO_3 (Chart 11)

Chart 11. Structure of [**12**]$^+$.

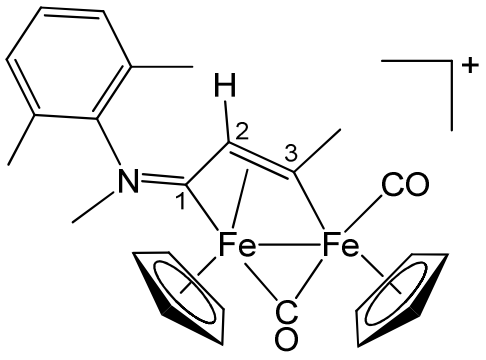

From [**1b**]CF_3SO_3 and propyne (in THF solution, ca. 1 mol/L). Brown solid, yield 85%. Anal. calcd. for $C_{26}H_{26}F_3Fe_2NO_5S$: C, 49.31; H, 4.14; N, 2.21. Found: C, 49.25; H, 4.28; N, 2.30. IR (CH_2Cl_2): ϋ/cm^{-1} = 2000vs (CO), 1815s (μ-CO), 1632m (C^2C^1N). ^1H NMR (dmso-d_6): δ/ppm = 7.23-7.18, 7.02-7.00 (m, 3 H, $C_6H_3Me_2$); 5.61, 5.33 (s, 10 H, Cp); 4.18 (s, 1 H, C^2H); 4.16 (s, 3 H, NMe); 3.77 (s, 3 H, C^3Me); 2.26, 1.72 (s, 6 H, $C_6H_3Me_2$). ^1H NMR (D_2O): δ/ppm = 7.37, 7.13, 6.95 (m, 3 H, $C_6H_3Me_2$); 5.40, 5.13 (s, 10 H, Cp); 4.10 (s, 3 H, NMe); 4.07 (s, 1 H, C^2H); 3.67 (s, 3 H, C^3Me); 2.17, 1.70 (s, 6 H, $C_6H_3Me_2$). ^{19}F NMR (D_2O): δ/ppm = −78.6. λ_{max}/nm (ε/$M^{-1}\cdot cm^{-1}$, CH_2Cl_2) = 223 ($6.1\cdot10^4$), 261 ($2.4\cdot10^4$), 314 ($1.7\cdot10^4$).

[$Fe_2Cp_2(CO)(\mu\text{-}CO)\{\mu\text{-}\eta^1\text{:}\eta^3\text{-}C^3(CH_2OH)C^2HC^1N(Me)(Xyl)\}$]$CF_3SO_3$, [13]$CF_3SO_3$ (Chart 12)

Chart 12. Structure of [**13**]$^+$.

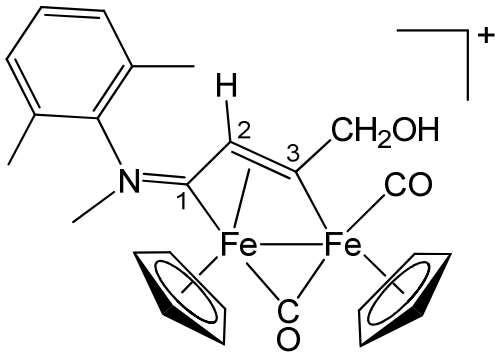

From [**1b**]CF_3SO_3 and propargyl alcohol. Dark brown solid, yield 80%. Anal. calcd. for $C_{26}H_{26}F_3Fe_2NO_6S$: C, 48.10; H, 4.04; N, 2.16. Found: C, 47.90; H, 3.95; N, 2.22. IR (CH_2Cl_2): ϋ/cm^{-1} = 2001vs (CO), 1810s (μ-CO), 1631m (C^2C^1N). ^1H NMR (dmso-d_6/D_2O 3:2): δ/ppm = 7.37, 7.14, 6.94 (m, 3 H, $C_6H_3Me_2$); 5.85, 5.62, *5.37*, *4.68* (m, 2 H, $^2J_{HH}$ = 16 Hz, CH_2); 5.44, 5.16 (s, 10 H, Cp); 4.60 (s, 1 H, C^2H); 4.07, *3.39* (s, 3 H, NMe); *2.35*, 2.15, *1.86*, 1.67 (s, 6 H, $C_6H_3Me_2$), E/Z ratio = 9. ^1H NMR (D_2O): δ/ppm = 7.41, 7.24, 7.17, 6.97 (m, 3 H, $C_6H_3Me_2$); 5.95-5.74 (m, 2 H, $^2J_{HH}$ = 16 Hz, CH_2); 5.43, *5.36*, 5.16 (s, 10 H, Cp); 4.12, *3.45* (s, 3 H, NMe); *2.40*, 2.17, *1.90*, 1.71 (s, 6 H, $C_6H_3Me_2$).

E/Z ratio = 7. ^{19}F NMR (D_2O): δ/ppm = –78.8. λ_{max}/nm (ε/$M^{-1}\cdot cm^{-1}$, CH_2Cl_2) = 226 ($4.1\cdot10^4$), 260 ($1.8\cdot10^4$), 309 ($1.4\cdot10^4$), 416 ($4.5\cdot10^3$).

$[Fe_2Cp_2(CO)(\mu\text{-}CO)\{\mu\text{-}\eta^1\text{:}\eta^3\text{-}C^3(3\text{-tiophenyl})C^2HC^1N(Me)(Xyl)\}]CF_3SO_3$, [14]$CF_3SO_3$ (Chart 13)

Chart 13. Structure of [**14**]$^+$.

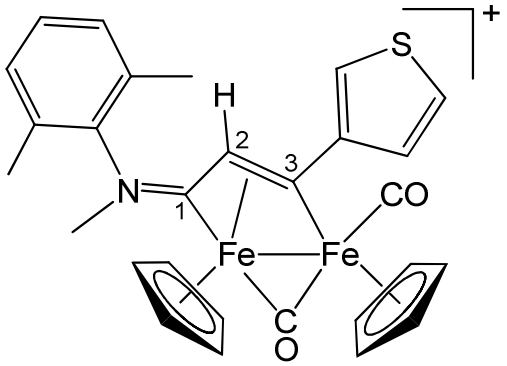

From [**1b**]CF_3SO_3 and 3-ethynylthiophene. Brown solid, yield 75%. Crystals suitable to X-ray analysis were obtained from a CH_2Cl_2 solution layered with Et_2O and stored at –30 °C. Anal. calcd. for $C_{29}H_{26}F_3Fe_2NO_5S_2$: C, 49.66; H, 3.74; N, 2.00. Found: C, 49.47; H, 3.67; N, 2.08. IR (CH_2Cl_2): ῡ/cm^{-1} = 2005vs (CO), 1818s (μ-CO), 1631m (C^2C^1N). IR (solid state): ῡ/cm^{-1} = 3112w, 2938w, 1995vs (CO), 1802s (CO), 1625m-s (C^2C^1N), 1584w, 1521vw, 1469w, 1435w, 1417w, 1263vs, 1223m-s, 1189w, 1146s, 1119m-sh, 1083w, 1064m, 1030vs, 1030vs, 1010m-sh, 961w, 859m, 843m-s, 780s, 752m, 737m-s, 705w, 682m, 654m. ^{1}H NMR (acetone-d_6): δ/ppm = 7.65-7.48, 7.26-7.08 (m, 6 H, C_4H_3S + $C_6H_3Me_2$); 5.62, 5.46, *5.41*, *5.02* (s, 10 H, Cp); 4.41, *3.72* (s, 3 H, NMe); 4.33 (s, 1 H, C^2H); 2.35, 1.88 (s, 6 H, $C_6H_3Me_2$), E/Z ratio = 9. $^{13}C\{^1H\}$ NMR (acetone-d_6): δ/ppm = 253.6 (*μ*-CO); 232.5 (C^1); 210.4 (CO); 200.2 (C^3); 157.1 (*ipso*-C_4H_3S); 145.4 (*ipso*-$C_6H_3Me_2$); 132.1, 131.3, 129.6, 129.3, 129.0 ($C_6H_3Me_2$); 126.3, 119.7 (C_4H_3S); 92.3, 88.2 (Cp); 53.2 (C^2); 45.6 (NMe); 17.3, 16.6 ($C_6H_3Me_2$). ^{1}H NMR (D_2O): δ/ppm = 9.37-7.13 (m, 6 H, C_4H_3S + $C_6H_3Me_2$); 5.36, 5.15 (s, 10 H, Cp); 4.15 (s, 3 H,

NMe); 2.31, 1.97 (s, 6 H, $C_6H_3Me_2$). ^{19}F NMR (D_2O): δ/ppm = –79.1. λ_{max}/nm (ε/$M^{-1}\cdot cm^{-1}$, CH_2Cl_2) = 227 ($4.3\cdot10^4$), 270 ($2.2\cdot10^4$), 300 ($1.6\cdot10^4$).

$[Fe_2Cp_2(CO)(\mu\text{-}CO)\{\mu\text{-}\eta^1\text{:}\eta^3\text{-}C^3(2\text{-naphthyl})C^2HC^1N(Me)(Xyl)\}]CF_3SO_3$, [15]$CF_3SO_3$ (Chart 14)

Chart 14. Structure of [**15**]$^+$.

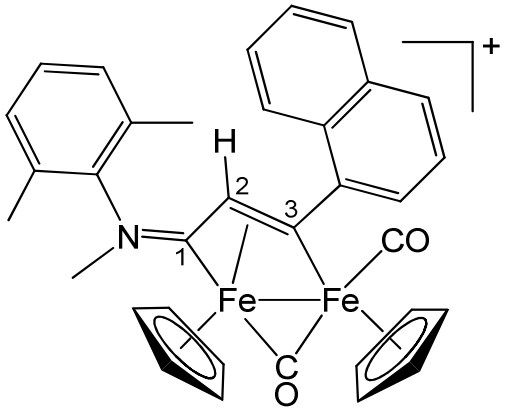

From [**1b**]CF_3SO_3 and 1-ethynylnaphthalene. Brown solid, yield 93%. Anal. calcd. for $C_{35}H_{30}F_3Fe_2NO_5S$: C, 56.40; H, 4.06; N, 1.88. Found: C, 56.30; H, 3.96; N, 1.96. IR (CH_2Cl_2): ϋ/cm^{-1} = 1998vs (CO), 1818s (μ-CO), 1627s (C^2C^1N). ^1H NMR (dmso-d_6): δ/ppm = 8.11-7.07 (m, 10 H, $C_{10}H_7$ + $C_6H_3Me_2$); 5.71, 5.21, *5.17*, *5.07* (s, 10 H, Cp); 4.29, *3.62* (s, 3 H, NMe); 4.24 (s, 1 H, C^2H); *2.46*, 2.16, *2.05*, 1.87 (s, 6 H, $C_6H_3Me_2$), E/Z ratio = 4. $^{13}C\{^1H\}$ NMR (dmso-d_6): δ/ppm = 255.1 (μ-CO); 232.1 (C^1); 211.9 (CO); 206.0 (C^3); 153.0 (*ipso*-$C_{10}H_7$); 145.7 (ipso-$C_6H_3Me_2$); 133.7, 132.1, 131.2, 129.8, 129.5, 129.0, 127.8, 126.6, 126.3, 126.0, 125.1, 124.8 ($C_{10}H_7$ + $C_6H_3Me_2$); 93.2, *93.1*, 89.1, *88.5* (Cp); 55.5 (C^2); *51.3*, 45.8 (NMe); *18.9*, 18.0, *17.8*, 17.3 ($C_6H_3Me_2$). ^1H NMR (D_2O): δ/ppm = 8.36-7.62 (m, 10 H, $C_{10}H_7$ + $C_6H_3Me_2$); *5.36*, *5.04*, 5.07, 4.98 (s, 10 H, Cp); 3.62 (s, 3 H, NMe); 2.88, *2.41*, 2.22, *2.02* (s, 6 H, $C_6H_3Me_2$), Z/E ratio = ca. 2. ^{19}F NMR (D_2O): δ/ppm = –79.1. λ_{max}/nm (ε/$M^{-1}\cdot cm^{-1}$, CH_2Cl_2) = 228 ($4.2\cdot10^4$), 313 ($1.3\cdot10^4$).

[$Fe_2Cp_2(CO)(\mu\text{-}CO)\{\mu\text{-}\eta^1\text{:}\eta^3\text{-}C^3(2\text{-pyridyl})C^2HC^1N(Me)(Xyl)\}]CF_3SO_3$, [16]$CF_3SO_3$ (Chart 15)

Chart 15. Structure of [**16**]$^+$.

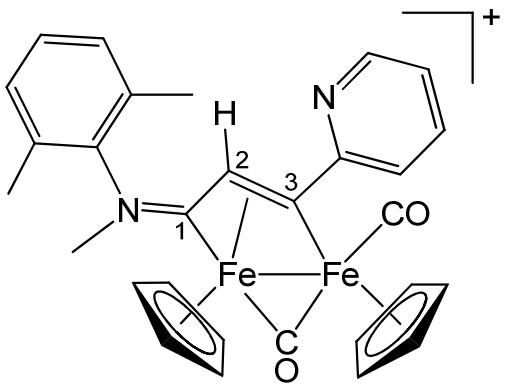

From [**1b**]CF_3SO_3 and 2-ethynylpyridine. Dark brown solid, yield 59%. Anal. calcd. for $C_{30}H_{27}F_3Fe_2N_2O_5S$: C, 51.75; H, 3.91; N, 4.02. Found: C, 51.93; H, 3.76; N, 4.09. IR (CH_2Cl_2): ϋ/cm^{-1} = 2003vs (CO), 1819s (μ-CO), 1631m (C^2C^1N). ^{1}H NMR (acetone-d_6): δ/ppm = 8.78, 7.89, 7.50-7.38, 7.27, 7.20, 7.10 (m, 7 H, C_5H_4N + $C_6H_3Me_2$); 5.64, 5.41, *5.37*, *5.07* (s, 10 H, Cp); 4.47 (s, 1 H, C^2H); 4.42, *3.76* (s, 3 H, NMe); *2.60*, 2.35, *2.09*, 1.89 (s, 6 H, $C_6H_3Me_2$), E/Z ratio = ca. 8. $^{13}C\{^1H\}$ NMR (dmso-d_6): δ/ppm = 253.3 (*μ*-CO); 232.7 (C^1); 210.3 (CO); 171.4 (C^3); 149.0, 145.3, 136.7, 132.1, 131.3, 129.6, 129.3, 122.0, 121.7 (C_5H_4N + $C_6H_3Me_2$); 91.9, *91.8*, 88.7, *88.2* (Cp); 53.1 (C^2); 45.8 (NMe); 17.3, 16.6 ($C_6H_3Me_2$). ^{1}H NMR (D_2O): δ/ppm = 8.62, 8.42, 8.01, 7.91, 7.77, 7.41, 7.34-6.99 (m, 7 H, C_5H_4N + $C_6H_3Me_2$); 5.38, 5.17, *5.12*, *4.89* (s, 10 H, Cp); 4.33 (s, 1 H, C^2H); 4.18, *3.54* (s, 3 H, NMe); *2.41*, 2.12, *1.94*, 1.75 (s, 6 H, $C_6H_3Me_2$), E/Z ratio = ca. 1.5. ^{19}F NMR (D_2O): δ/ppm = –78.9. λ_{max}/nm (ε/$M^{-1}\cdot cm^{-1}$, CH_2Cl_2) = 228 ($4.2\cdot10^4$), 271 ($2.2\cdot10^4$), 323 ($1.3\cdot10^4$).

[$Fe_2Cp_2(CO)(\mu\text{-}CO)\{\mu\text{-}\eta^1\text{:}\eta^3\text{-}C^3(CO_2Me)C^2(CO_2Me)C^1N(Me)(Xyl)\}]CF_3SO_3$, [17]$CF_3SO_3$ (Chart 16)

Chart 16. Structure of [**17**]$^+$.

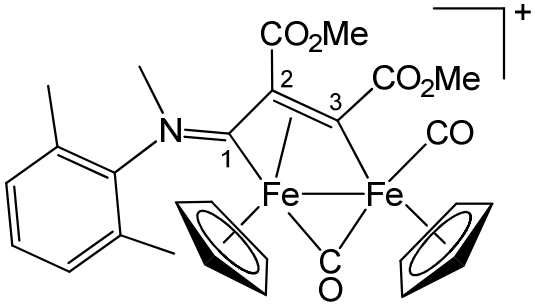

From [**1b**]CF_3SO_3 and dimethyl acetylenedicarboxylate. Dark orange solid, yield 82%. Anal. calcd. for $C_{29}H_{28}F_3Fe_2NO_9S$: C, 47.37; H, 3.84; N, 1.90. Found: C, 47.12; H, 3.75; N, 1.98. IR (CH_2Cl_2): $\tilde{\upsilon}/cm^{-1}$ = 2007vs (CO), 1843s (μ-CO), 1733m (CO_2Me), 1717m (CO_2Me), 1629m (C^2C^1N). ^1H NMR (dmso-d_6/D_2O 1:1): δ/ppm = 7.40, 7.21 (m, 3 H, $C_6H_3Me_2$); 5.32, 4.86 (s, 10 H, Cp); 4.06, 3.83 (s, 6 H, CO_2Me); 3.44 (s, 3 H, NMe); 2.44, 1.87 (s, 6 H, $C_6H_3Me_2$). ^1H NMR (D_2O): δ/ppm = 7.42, 7.2-7.0 (m, 3 H, $C_6H_3Me_2$); 5.34, 4.91 (s, 10 H, Cp); 4.13, 3.89 (s, 6 H, CO_2Me); 3.51 (s, 3 H, NMe); 2.47, 1.90 (s, 6 H, $C_6H_3Me_2$). ^{19}F NMR (D_2O): δ/ppm = –78.9. λ_{max}/nm ($\varepsilon/M^{-1}\cdot cm^{-1}$, CH_2Cl_2) = 225 ($4.1\cdot10^4$), 295 ($1.4\cdot10^4$), 404 ($4.1\cdot10^3$).

[Fe_2Cp_2(CO)(μ-CO){μ-η^1:η^3-C^3(Me)C^2(Me)C^1N(Me)(Xyl)}]CF_3SO_3, [18]CF_3SO_3 (Chart 17)

Chart 17. Structure of [**18**]$^+$.

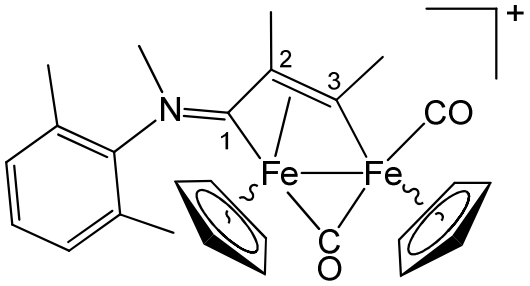

Trans-[**18**]CF_3SO_3. From [**1b**]CF_3SO_3 and 2-butyne (ca. 3 equivalents). Dark green solid, yield 76%. Anal. calcd. for $C_{27}H_{28}F_3Fe_2NO_5S$: C, 50.10; H, 4.36; N, 2.16. Found: C, 49.87; H, 4.47; N, 2.24. IR

(CH_2Cl_2): $\tilde{\upsilon}$/cm^{-1} = 1985vs (CO), 1823s (μ-CO), 1610m (C^2C^1N). ^{1}H NMR (dmso-d_6): δ/ppm = 7.43, 7.35, 7.12, 6.90 (m, 3 H, $C_6H_3Me_2$); 5.56, 4.88 (s, 10 H, Cp); 3.99 (s, 3 H, C^3Me); 3.56 (s, 3 H, NMe); 2.61, 2.06 (s, 6 H, $C_6H_3Me_2$); 2.22 (s, 3 H, C^2Me). λ_{max}/nm (ε/$M^{-1}\cdot cm^{-1}$, CH_2Cl_2) = 224 ($3.7\cdot10^4$), 264 ($1.6\cdot10^4$), 292 ($1.3\cdot10^4$).

Cis-[**18**]CF_3SO_3. This compound was obtained by heating a solution of *trans*-[**18**]CF_3SO_3 (ca. 0.40 mmol) in methanol (15 mL), under nitrogen, for 3 hours. The final brown-red solution was dried under reduced pressure, the residue was dissolved into a small volume of CH_2Cl_2 and charged on alumina. Impurities were separated by using CH_2Cl_2/THF mixtures and neat THF as eluent. The product was obtained by using MeOH as eluent as a red fraction, which was dried under vacuum. Dark red solid, yield 91%. Anal. calcd. for $C_{27}H_{28}F_3Fe_2NO_5S$: C, 50.10; H, 4.36; N, 2.16. Found: C, 49.78; H, 4.35; N, 2.20. IR (CH_2Cl_2): $\tilde{\upsilon}$/cm^{-1} = 1987vs (CO), 1819s (μ-CO), 1610m (C^2C^1N). ^{1}H NMR (acetone-d_6): δ/ppm = 7.48, 7.35 (m, 3 H, $C_6H_3Me_2$); 5.57, 4.88 (s, 10 H, Cp); 4.01 (s, 3 H, C^3Me); 3.57 (s, 3 H, NMe); 2.61, 2.06 (s, 6 H, $C_6H_3Me_2$); 2.25 (s, 3 H, C^2Me). ^{1}H NMR (D_2O): δ/ppm = 7.38, 7.20, 7.12, 6.89, 6.82 (m, 3 H, $C_6H_3Me_2$); 5.29, 4.66 (s, 10 H, Cp); 3.77 (s, 3 H, C^3Me); 3.36 (s, 3 H, NMe); 2.41, 1.90 (s, 6 H, $C_6H_3Me_2$); 2.02 (s, 3 H, C^2Me). λ_{max}/nm (ε/$M^{-1}\cdot cm^{-1}$, CH_2Cl_2) = 226 ($4.0\cdot10^4$), 265 ($2.0\cdot10^4$), 302 ($1.7\cdot10^4$).

$[Fe_2Cp_2(CO)(\mu\text{-}CO)\{\mu\text{-}\eta^1\text{:}\eta^3\text{-}C^3(Ph)C^2HC^1N(Me)(CH_2Ph)\}]CF_3SO_3$, [19]$CF_3SO_3$ (Chart 18).

Chart 18. Structure of [**19**]$^+$.

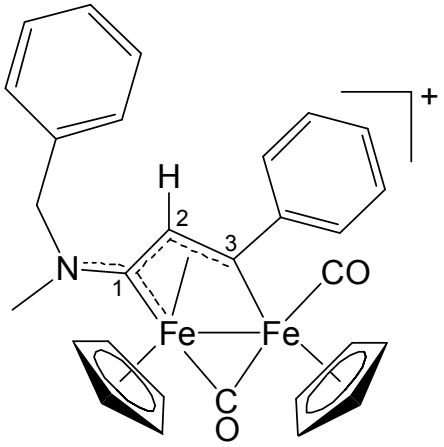

From [**1c**]CF_3SO_3 and phenylacetylene. Brown solid, yield 72%. Anal. calcd. for $C_{30}H_{26}F_3Fe_2NO_5S$: C, 52.89; H, 3.85; N, 2.06. Found: C, 52.74; H, 3.96; N, 2.02. IR (CH_2Cl_2): $\tilde{\upsilon}$/cm^{-1} = 1991vs (CO), 1809s (μ-CO), 1666m (C^2C^1N). ^{1}H NMR (acetone-d_6): δ/ppm = 7.89-7.36 (Ph); *5.50*, 5.48, *5.32*, 5.30 (s, Cp); 5.72, 5.41, *5.00*, *4.82* (d, $^2J_{HH}$ = 14 Hz, C*H*$_2$Ph); 4.77 (s, C^2H); 3.94, *3.20* (s, NMe). E/Z ratio = 1.6. ^{13}C{^{1}H} NMR (acetone-d_6): δ/ppm = *257.6*, 256.1 (μ-CO); 226.4, *226.1* (C^1); 210.4, 210.3 (CO); *204.9*, 204.4 (C^3); 156.5 (*ipso*-PhCH$_2$); 133.4, 132.8 (*ipso*-Ph); 128.8, 129.7, 129.5, 129.4, 129.1, 128.9, 128.5, 127.7, 127.0 (Ph); 92.0, 88.4, 88.3 (Cp); 68.1, *61.5* (*C*H$_2$Ph); 53.4, 53.3 (C^2); *47.9*, 42.4 (NMe). ^{19}F NMR (D_2O): δ/ppm = –78.9.

Synthesis and characterization of [FeCp(CO){C^1N(Me)(Xyl)C^2HC^3(Ph)C(=O)}], 21c (Chart 19)

Chart 19. Structure of **21c**.

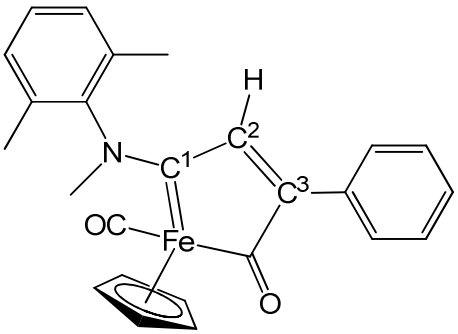

Compound [**11**]CF_3SO_3 (280 mg, 0.403 mmol) was dissolved in tetrahydrofuran (15 mL), then $CoCp_2$ (99 mg, 0.52 mmol) was added. The mixture was stirred at room temperature overnight, then it was passed through a short alumina pad using neat acetonitrile as eluent. The filtrated solution was dried under vacuum. The residue was dissolved in diethyl ether/dichloromethane mixture (1:1 v/v) and charged on alumina column. Elution with petroleum ether/diethyl ether mixtures allowed the removal of impurities, then the fraction corresponding to **21c** was collected with neat diethyl ether. Removal of the solvent under vacuum afforded the title product as a brown, air stable solid. Yield 84% (respect to $C^1C^2C^3$ chain). Anal. calcd. for $C_{25}H_{23}FeNO_2$: C, 70.60; H, 5.45; N, 3.29. Found: C, 70.44; H, 5.57; N, 3.14. IR (CH_2Cl_2): ϋ/cm^{-1} = 1919vs (CO), 1612m (CO_{acyl}), 1571m (C^1N). IR (solid state): ϋ/cm^{-1} = 3082w, 3029w, 2925w, 1907vs, 1614m (CO_{acyl}), 1571w-m (C^1N), 1471m, 1383m, 1352w, 1299w, 1084s-br, 1015s-br, 879w, 798vs, 774vs, 719w, 696m, 656w. ^{1}H NMR (acetone-d_6): δ/ppm = 7.38-7.22 (m, 8 H, $C_6H_3Me_2$ + Ph); 6.96 (s, 1 H, C^2H); 4.73 (s, 5 H, Cp); 3.96 (s, 3 H, NMe); 2.32, 2.17 (s, 6 H, $C_6H_3Me_2$). $^{13}C\{^1H\}$ NMR (acetone-d_6): δ/ppm = 264.7, 264.6 (CO_{acyl} + C^1); 221.9 (CO); 168.7 (C^3); 147.5 (C^2); 145.5 (*ipso*-C_6H_3); 132.9, 132.7, 132.4, 129.1, 129.0, 128.9, 128.8, 128.7, 127.9 ($C_6H_3Me_2$ + Ph); 85.1 (Cp); 48.8 (NMe); 17.0, 16.6 ($C_6H_3Me_2$). Crystallization from a diethyl ether solution layered with pentane and stored at –30 °C afforded dark brown crystals of **21c**.

2. Solubility and stability in aqueous media

a) Solubility in D_2O. Each compound ([**2-19**]CF_3SO_3, ca. 0.05 mmol) was added to a D_2O solution (0.7 mL) of Me_2SO_2 (c = $7.1\cdot10^{-3}$ mol·L^{-1}), and the resulting mixture was stirred at 21 °C for 8 hours. The saturated solution was filtrated and transferred into an NMR tube, then analyzed by ^{1}H NMR spectroscopy. The concentration (i.e. solubility) was calculated by the relative integral with respect to Me_2SO_2 as internal standard [δ/ppm = 3.14 (s, 6H) in D_2O)]. Solubility data in D_2O for [**2-19**]CF_3SO_3 are compiled in Table 1.

b) Stability in D_2O or D_2O/DMSO-d_6 solutions. A mixture of the selected Fe compound ([**2-19**]CF_3SO_3, *ca*. 4 mg) and D_2O (0.9 mL) was stirred at room temperature for 30 minutes, and then filtered over celite and transferred into an NMR tube. D_2O/DMSO-d_6 mixtures were used for compounds with low water solubility (7:1 *v*/*v* for [**13**]$^+$; 3:1 *v*/*v* for [**12**]$^+$, [**14**]$^+$; 1:1 *v*/*v* for [**10**]$^+$, [**15**]$^+$). The resulting solutions were analyzed by ^{1}H NMR and then heated at 37 °C for 72 hours. After cooling to room temperature, the final solutions were separated from a minor amount of brown precipitate by filtration over celite, and analyzed by ^{1}H NMR: in general, the resonances due to the starting material were clearly detected, together with minor additional signals which could not be assigned (3.8-1.0 ppm). No other Fe-cyclopentadienyl species was found in solution. The precipitate (ca. 1.3 mg) obtained from [**7**]CF_3SO_3 (20 mg) was analyzed by Raman spectroscopy and identified as hematite (Raman shifts: 216, 284, 394 cm^{-1}). NMR data for the tested compounds are given in the SI. For D_2O/DMSO-d_6 mixtures, ^{1}H chemical shift values are referenced to the DMSO-d_6 residual peak as in pure D_2O (δ/ppm = 2.71). The stability experiments were repeated with the addition of NaCl up to ca. 0.1 M concentration, giving substantially analogous results.

c) Stability in cell culture medium. Each compound ([**2-19**]CF_3SO_3, ca. 0.01 mmol) was dissolved in dmso (ca. 0.2 mL) in a glass tube, then 3 mL of RPMI-1640 medium (Merck; modified with sodium bicarbonate, without L-glutamine and phenol red, liquid, sterile-filtered, suitable for cell culture) were added. Compound **21c** was dissolved in 1 mL dmso. The resulting mixture was maintained at 37 °C for 72 h, then allowed to cool to room temperature and extracted with CH_2Cl_2 (7 mL). The organic phase was analyzed by IR spectroscopy (CH_2Cl_2 solution), cleanly showing the bands of the starting compound only, with the exception of the sample derived from [**17**]CF_3SO_3 (appearance of additional, intense band at 1629 cm^{-1}). For those compounds that could not be efficiently recovered with CH_2Cl_2 extraction, an aliquot of the aqueous phase was analyzed by mass spectrometry in positive ion scan mode with an API 4000 instrument (SCIEX), equipped with an electrospray source. The mass spectra

evidenced the presence of the diiron vinyliminium cation as the largely prevalent species ([**5**]$^+$: 500.1; [**12**]$^+$: 484.2; [**13**]$^+$: 500.3 m/z), with the exception of the sample derived from [**8**]CF_3SO_3 (prevalent peak at 438.2 m/z).

3. Determination of partition coefficients (Log P_{ow})

Partition coefficients (P_{ow}; IUPAC: K_D partition constant[54]), defined as $P_{ow} = c_{org}/c_{aq}$, where c_{org} and c_{aq} are the molar concentrations of the selected compound in the organic and aqueous phases, respectively, and were determined by the shake-flask method and UV-Vis measurements.[34] Values of Log P_{ow} for [**2-19**]CF_3SO_3 are compiled in Table 1. All the operations were carried out at 21±1°C. De-ionized water and 1-octanol were mixed and vigorously stirred for 24 hours at room temperature to allow saturation of both phases, then separated by centrifugation and used for the following experiments. A solution of the selected Fe compound ([**2-19**]CF_3SO_3) in the aqueous phase (V = 10 mL) was prepared and its UV-Vis spectrum was recorded. An aliquot of the solution (V_{aq} = 3.0 mL) was then transferred into a test tube and the organic phase ($V_{org} = V_{aq}$ = 3.0 mL) was added. The mixture was vigorously stirred for 2 h and the resulting emulsion was centrifuged (2000 rpm, 15'). Hence the UV-Vis spectrum of the aqueous phase was recorded. The partition coefficient was then calculated as $P_{ow} = \frac{A_{0,aq} - A_{aq}}{A_{aq}}$, where $A_{0,aq}$ and A_{aq} are the absorbance in the aqueous phase respectively before and after mixing with the organic phase.[34] UV-Vis measurements were carried out using 1 cm quartz cuvettes. The wavelength of the maximum absorption of each compound was used for UV-Vis quantification.

4. Electrochemistry

Cyclic voltammetry measurements were performed with a PalmSens4 instrument interfaced to a computer employing PSTrace5 electrochemical software. All potentials are reported *vs.* $FeCp_2$. Current sign convention adopted: negative, currents/cathodic process; positive, currents/anodic process.

Experiments in aqueous media. Phosphate buffer (PB) solution (Na_2HPO_4/KH_2PO_4, $\Sigma c_{(PO4)}$ = 50 mM, pH = 7.3) was prepared with ultrapure H_2O and used as supporting electrolytes. $[FeCp_2]PF_6$ (Sigma Aldrich) was used without further purification. The three-electrode home-built cell was equipped with a Pt sheet counter electrode, teflon-encapsulated glassy-carbon (GC) working electrode (BASi, ø 3 mm) and a quasi-reference Pt electrode. Prior to measurements, the working GC electrode was polished by the following procedure:[55] manual rubbing with 0.3 μM Al_2O_3 slurry in water (eDAQ) for 2 min, then sonication in ultrapure water for 10 min, manual rubbing with 0.05 μM Al_2O_3 slurry in water (eDAQ) for 2 min, then sonication in ultrapure water for 10 min.

The supporting electrolyte (5.0 mL) was introduced into the cell and deaerated by bubbling argon for 2-3 minutes. The CV of the solvent was recorded. The analyte was then introduced ($c \approx 7 \cdot 10^{-4}$ M) and voltammograms were recorded (0.1 V/s); a small amount of $[FeCp_2]PF_6$ was added to the solution, and a further voltammogram was repeated. Under the present experimental conditions, the one-electron reduction of ferrocenium occurred at E° = +0.41 V *vs* NHE.

Experiments in organic solvents. HPLC grade THF (Sigma Aldrich) was distilled from CaH_2 and stored under Ar over 3Å molecular sieves. $[N^nBu_4]PF_6$ (Fluka, electrochemical grade) and Cp_2Fe (Fluka) were used without further purification. CV measurements were carried out under Ar using 0.2 M $[N^nBu_4]PF_6$ in THF as the supporting electrolyte. The working and the counter electrodes consisted of a Pt disk and a Pt gauze, respectively, both sealed in a glass tube. A quasi-reference Pt electrode was employed as a reference. The three-electrode home-built cell was pre-dried by heating under vacuum and filled with argon. The Schlenk-type construction of the cell maintained anhydrous and anaerobic conditions. The solution of supporting electrolyte, prepared under argon, was introduced into the cell

and the CV of the solvent was recorded. The analyte was then introduced (c ≈ $7 \cdot 10^{-4}$ M) and voltammograms were recorded (0.1 V/s); a small amount of ferrocene was added to the solution, and a further voltammogram repeated. Under the present experimental conditions, the one-electron reduction of ferrocene occurred at E° = +0.59 V *vs* SCE.

Infrared (IR) spectro-electrochemical measurements were carried out using an optically transparent thin-layer electrochemical (OTTLE) cell equipped with CaF_2 windows, platinum mini-grid working and auxiliary electrodes and silver wire pseudo-reference electrode.[56] During the microelectrolysis procedures, the electrode potential was controlled by a PalmSens4 instrument interfaced to a computer employing PSTrace5 electrochemical software. Argon-saturated THF solutions of the analyzed compound, containing $[N^nBu_4]PF_6$ 0.2 M as the supporting electrolyte, were used. The *in situ* spectroelectrochemical experiments were performed by collecting IR spectra at fixed time intervals during the oxidation or reduction, obtained by continuously increasing or lowering the initial working potential at a scan rate of 2.0 mV/sec. IR spectra were recorded on a Perkin-Elmer FT-IR 1725X spectrophotometer and UV-Vis spectra on a Perkin-Elmer Lambda EZ201 spectrophotometer.

5. X-ray crystallography

Crystal data and collection details for [**10**]CF_3SO_3, [**14**]$CF_3SO_3 \cdot 0.5CH_2Cl_2$, [**15**]$CF_3SO_3 \cdot CH_2Cl_2$, [**16**]$CF_3SO_3 \cdot 0.5CH_2Cl_2$ and **21c** are reported in Table S4. Data were recorded on a Bruker APEX II diffractometer equipped with a PHOTON100 detector using Mo–Kα radiation. Data were corrected for Lorentz polarization and absorption effects (empirical absorption correction SADABS).[57] The structures were solved by direct methods and refined by full-matrix least-squares based on all data using F^2.[58] Hydrogen atoms were fixed at calculated positions and refined by a riding model. All non-hydrogen atoms were refined with anisotropic displacement parameters.

6. Cell culture and cytotoxicity studies

Human ovarian carcinoma (A2780 and A2780cisR) cell lines were obtained from the European Collection of Cell Cultures (ECACC, UK). The non-tumoral human embryonic kidney (HEK-293) cell line was obtained from ATCC (Sigma, Switzerland). RPMI-1640 GlutaMAX and DMEM GlutaMAX media were obtained from Life Technologies (Switzerland), fetal bovine serum (FBS) was obtained from Sigma, penicillin streptomycin solution was obtained from Life Technologies and cisplatin was obtained from TCI.

The cells were routinely cultured in RPMI-1640 GlutaMAX (A2780 and A2780cisR) and DMEM GlutaMAX (HEK-293) medium containing 10% heat-inactivated FBS and 1% penicillin/streptomycin solution at 37 °C and CO_2 (5%). The A2780cisR cell line was routinely treated with cisplatin (2 μM) in the medium. The cytotoxicity of the compounds was determined using the MTT assay (MTT = 3-(4,5-dimethyl-2-thiazolyl)-2,5-diphenyl-2H-tetrazolium bromide).[59] Cells were seeded in flat-bottom 96-well plates as a suspension in medium containing 10% heat-inactivated FBS and 1% penicillin/streptomycin solution (100 μL and approximately 4300 cells per well) and incubated for 24 h. Stock solutions of compounds were prepared in DMSO and were rapidly diluted in medium. The solutions were sequentially diluted (final DMSO concentration of 0.5%) to give a compound concentration range (0 μM to 500 μM). Cisplatin was included as a positive control (0 μM to 100 μM). The compounds were added to the pre-incubated 96-well plates in 100 μL aliquots and the plates were incubated for 72 hours. For selected compounds undergoing ROS determination, the IC_{50} value was also assessed after 24 hours of incubation. MTT (20μL, 5 mg/mL in Dulbecco's Phosphate Buffered Saline, DPBS) was added to the cells and the plates were incubated for further 4 h. The culture medium was aspirated, and the purple formazan crystals formed by the mitochondrial dehydrogenase activity of vital cells were dissolved in DMSO (100 μL per well). The absorbance of the resulting solutions, directly proportional to the number of surviving cells, was quantified at 590 nm using a SpectroMax

M5e multi-mode microplate reader (using SoftMax Pro software, version 6.2.2). The percentage of surviving cells was calculated from the absorbance of wells corresponding to the untreated control cells. The reported IC50 values (Table 4) are based on means from two independent experiments, each comprising four testings per concentration level.

7. ROS determination

The intracellular increase of reactive oxygen species (ROS) upon treatment of the analyzed complexes was measured by using the DCFH-DA (2′,7′-dichlorodihydrofluorescein diacetate, Sigma Aldrich) assay, based on cellular uptake of the non-fluorescent diacetate following deacetylation by esterases (2′,7′-dichlorodihydrofluorescein, DCFH) and oxidation to the fluorescent dichlorofluorescein (2′,7′-dichloro-fluorescein, DCF).[60] Thus, A2780 and A2780cisR cells were seeded at concentration of $4 \cdot 10^4$ cells/well/90 μL of complete growth medium into 96-well plates. After overnight incubation, the cells were treated following manufacturer protocol. The culture medium was supplemented with 100 μL of a solution containing the fluorogenic probe and cells were incubated with 5% CO_2 at 37 °C. After 1 h, cells were exposed with a final concentration of 100 μM of the tested compound and 5% CO_2 at 37 °C; the same concentration of H_2O_2 was used as a positive control. Stock solutions of compounds were prepared as described above; cells incubated with equal amounts of DMSO in supplemented RPMI were used as control. The fluorescence was measured up to 24 hours with an excitation wavelength of 485 nm and with a 535 nm emission filter by Multilabel Counter (PerkinElmer, Waltham, USA). The analyses were conducted on triplicate and experimental data were reported as mean ± SD. Statistical differences were analyzed using one-way analysis of variance (ANOVA), and a Tukey test was used for post hoc analysis. A p-value <0.05 was considered statistically significant.

8. Interaction with biomolecules

Guanosine 5'-monophosphate disodium salt hydrate (Merck), amyloid β-protein (residues 1-16, H-Asp-Ala-Glu-Phe-Arg-His-Asp-Ser-Gly-Tyr-Glu-Val-His-His-Gln-Lys-OH) as its trifluoroacetate salt (Bachem), ubiquitin from bovine erythrocytes (Merck), bovine serum albumin (BSA, crystallized and lyophilized powder) and 14-mer oligonucleotide 5'-ATACATGGTACATA-3' (Microsynth) were received from commercial suppliers. The latter species was desalted with five rounds of centrifugation using 3 kDa-cutoff Amicon Ultra centrifugal filters, according to manufacturer's instructions. Solutions of each of these biomolecules (100 to 500 μM) were incubated with [**7**]CF_3SO_3 in 1:1 to 1:10 ratio at 37 °C for 24 h. Analogous solutions of BSA were incubated with [**2**,**7**,**10**,**11**]CF_3SO_3 in 1:1 ratio at 37 °C for 24 h. All incubations were performed in sterile MilliQ water (samples for mass spectrometry analysis) or D_2O (samples for NMR analysis). Mass spectrometry measurements were performed either with LTQ Orbitrap Elite (Thermo Fischer) or with API 4000 instrument (SCIEX) equipped with an Ionspray/APCI source. When necessary, samples were stored at –20 °C prior to analysis.

Fluorescence measurements were performed on a Perkin Elmer PE spectrofluorometer with temperature control (± 0.1 °C). Calf-thymus DNA (B-double helix, highly polymerized salt) and ethidium bromide (EB) were received from Merck. Calf-thymus DNA was sonicated to reduce its length to ca. 500 base pairs.[61] The concentrations of DNA (C_{DNA}, referred to base pairs; $\lambda = 260$ nm, $\varepsilon = 13200\ M^{-1} \cdot cm^{-1}$),[62] EB ($C_{EB}$;$\lambda = 480$ nm, $\varepsilon = 5700\ M^{-1} \cdot cm^{-1}$)[63] and BSA ($C_{BSA}$; $\lambda = 278$ nm, $\varepsilon = 44000\ M^{-1} \cdot cm^{-1}$) [64] were determined spectrophotometrically. The solutions were prepared with ultra-pure water (Sartorius). A sodium cacodylate (NaCac) buffer was used to keep pH of solutions at 7.0, whereas NaCl was used to adjust the ionic strength close to physiological conditions (0.1 M). For EB/DNA exchange experiments, a stock $1.73 \cdot 10^{-4}$ M solution (NaCac 0.01 M, NaCl 0.1 M, pH = 7.0) was used to titrate a $2.14 \cdot 10^{-4}$ M solution of DNA directly into the spectrofluorometric cell. Additions of the titrant were carried out with a Gastight syringe connected to a Mitutoyo screw (minimum amount = 0.164 μL). The DNA was saturated (and EB addition was

stopped) when the fluorescence emission increase faded out (T = 25 °C, $C_{DNA}/C_{EB} \cong 2$, λ_{exc} = 520 nm, λ_{em} = 530-650 nm, λ_{em}^{MAX} = 595 nm). After DNA saturation, increasing amounts of the analyzed metal complex were added to the EB/DNA mixture. Fluorescence changes were measured at the excitation/emission wavelength typical and selective for the EB/DNA intercalated complex (λ_{exc} = 520 nm, λ_{em} = 595 nm). The blank test was done by adding DMSO only to the EB/DNA mixture, in order to quantify fluorescence changes due to solvent and dilution effects. In the case of direct metal complex/BSA fluorescence titrations, a similar procedure was used, thus the analyzed metal complex (ca. 10^{-3} M, DMSO solution) was added to 10^{-6} M BSA solutions (NaCac 0.01 M, NaCl 0.1 M, pH = 7.0). The volumes of the added solutions of metal complexes are so small to ensure negligible presence of DMSO in the system.

Acknowledgements

We gratefully thank the University of Pisa (PRA_2017_25, "*composti di metalli di transizione come possibili agenti antitumorali"*) and the Swiss National Science Foundation for financial support. Dr. Beatrice Campanella (ICCOM – CNR, Pisa, Italy) is acknowledged for executing the Raman analysis.

Supporting Information Available

NMR spectra (Figures S1-S37), X-ray structures (Figures S38-S40 and Tables S1, S4), electrochemical voltammograms (Figures S41-S44), spectro-electrochemical studies (Figures S45-S48 and Table S2), BSA binding studies (Figures S49-S51 and Table S3). CCDC reference numbers 1906548 ([**14**]CF_3SO_3), 1906549 ([**15**]CF_3SO_3), 1906550 ([**16**]CF_3SO_3) and 1906551 (**21c**) contain the supplementary crystallographic data for the X-ray studies reported in this paper. These data can be obtained free of charge at www.ccdc.cam.ac.uk/conts/retrieving.html (or from the Cambridge

Crystallographic Data Centre, 12, Union Road, Cambridge CB2 1EZ, UK; fax: (internat.) +44-1223/336-033; e-mail: deposit@ccdc.cam.ac.uk).

References

1 a) N. P. E. Barry, P. J. Sadler, Chem. Commun. 2013, 49, 5106-5131. b) A.-L. Lainé, C. Passirani, Curr. Opin. Pharmacol. 2012, 12, 420–426. c) U. Jungwirth, C. R. Kowol, B. K. Keppler, C. G. Hartinger, W. Berger, P. Heffeter, Antioxid Redox Signal. 2011, 15, 1085-1127.

2 a) D. Gibson, Dalton Trans., 2009, 10681–10689. b) M. S. Robilalrd, J. Reedijk, Encyclopedia of Inorganic and Bioinorganic Chemistry, Leiden University, 2011, 1-11. c) M. G Apps, E. H. Y. Choi, N. J Wheate, Endocrine-Related Cancer 2015, 22, R219–R233. d) S. Dasari, P. B. Tchounwou, Eur. J. Pharmacol. 2014, 740, 364-378.

3 a) R. Oun, Y. E. Moussa, N. J. Wheate, Dalton Trans., 2018, 47, 6645–6653. b) Y. Min, C.-Q. Mao, S. Chen, G. Ma, J. Wang, Y. Liu, Angew. Chem. 2012, 124, 6846-6851.

4 a) T. C. Johnstone, K. Suntharalingam, S. J. Lippard, Chem. Rev. 2016, 116, 3436-3486. b) P. Zhang, P. J. Sadler, J. Organomet. Chem. 2017, 839, 5-14. c) C. S. Allardyce, P. J. Dyson, Dalton Trans., 2016, 45, 3201-3209. d) N. P. E. Barry, P. J. Sadler, Chem. Commun., 2013, 49, 5016-5041. e) M. Marloye, G. Berger, M. Gelbcke, F. Dufrasne, Future Med. Chem. 2016, 8, 2263-2286. f) I. Bratsos, T. Gianferrara, E. Alessio, C. G. Hartinger, M. A. Jakupec, B. K. Keppler, Bioinorganic Medicinal Chemistry, ed. E. Alessio, Wiley-VCH, Weinheim, 2011, 151-174. g) P. Štarha, Z. Trávníček, Coord. Chem. Rev. 2019, 395, 130–145. h) C. Santini, M. Pellei, V. Gandin, M. Porchia, F. Tisato, C. Marzano, Chem. Rev. 2014, 114, 815-862. i) M. N. Alam, F. Huq, Coord. Chem. Rev. 2016, 316, 36–67. j) R Alberto, C Biot, A Casini, D Dive, PJ Dyson, S Gibaud, A Habtermariam, CG Hartinger, EA Hillard, M Hogan, G Jaouen, BE Mann, E Meggers, SP Mulcahy, AA Nazarov, N Metzler-Nolte, AM Pizarro, PJ Sadler, M Tacke, A Vessieres, Topics in Organometallic Chemistry, 2010, Vol. 32.

5 a) T. C. Johnstone, K. Suntharalingam, S. J. Lippard, Chem. Rev. 2016, 116, 3436-3486. b) X. Wang, X. Wang, Z. Guo, Acc. Chem. Res. 2015, 48, 2622−2631. c) L. Bai, C. Gao, Q. Liu, C. Yu, Z. Zhang, L. Cai, B. Yang, Y. Qian, J. Yang, X. Liao, Eur. J. Med. Chem. 2017, 140, 349-382. d) P. Štarha, J. Vančo, Z. Trávníček, Coord. Chem. Rev. 2019, 380, 103–135. e) D. Gibson, J. Inorg. Biochem. 2019, 191, 77–84. e) Z. Wang, Z. Deng, G. Zhu, Dalton Trans., 2019, 48, 2536–2544. f) K. Mitra, Dalton Trans., 2016, 45 , 19157–19171.

6 a) E. Y. Tshuva, J. A. Ashenhurst, Eur. J. Inorg. Chem. 2009, 2203–2218. b) E. Y. Tshuva, D. Peri, Coord. Chem. Rev. 2009, 253, 2098–2115. c) J. Ceballos-Torres, P. Virag, M. Cenariu, S. Prashar, M. Fajardo, E. Fischer-Fodor, S. Gomez-Ruiz, Chem. Eur. J. 2014, 20, 10811-10828. d) M. Picquet, M. Wenzel, B. Bertrand, P. Richard, P. Le Gendre, A. Casini, A. Nazarov, M. Groessl, O. Zava, J. Biol. Inorg. Chem. 2014, 19, S646-S646.

7 a) S. Thota, D. A. Rodrigues, D. C. Crans, E. J. Barreiro, J. Med. Chem. 2018, 61, 5805-5821. b) L. Zeng, P. Gupta, Y. Chen, E. Wang, L. Ji, H. Chao, Z.-S. Chen, Chem. Soc. Rev., 2017, 46, 5771-5804. c) E. Alessio, Eur. J. Inorg. Chem. 2017, 1549–1560. d) A. Weiss, R. H. Berndsen, M. Dubois, C. Müller, R. Schibli, A. W. Griffioen, P. J. Dyson, P. Nowak-Sliwinska, Chem. Sci., 2014, 5 , 4742–4748. e) S. M. Meier-Menches, C. Gerner, W. Berger, C. G. Hartinger, B. K. Keppler, Chem. Soc. Rev., 2018, 47, 909-928. f) S. M. Meier-Menches, C. Gerner, W. Berger, C. G. Hartinger, B. K. Keppler, Chem. Soc. Rev., 2018, 47, 909-928. g) A. A. Nazarov, C. G. Hartinger, P. J. Dyson, J. Organomet. Chem. 2014, 751, 251-260.

8 a) B. Bertrand, M. A. O'Connell, Z. A. E. Waller, M. Bochmann, Chem. Eur. J. 2018, 24, 3613-3622. b) T. Zou, C. T. Lum, C.-N. Lok, J.-J. Zhang, C.-M. Che, Chem. Soc. Rev., 2015, 44, 8786-8801. c) M. P. Chrysouli, C. N. Banti, N. Kourkoumelis, N. Panayiotou, G. S. Markopoulos, A. J. Tasiopoulos, S. K. Hadjikakou, J. Inorg. Biochem. 2018, 179, 107–120. d) M. Mora, M. C. Gimeno, R. Visbal, Chem. Soc. Rev. 2019, 48, 447-462. e) T. Lazarevi, A. Rilak, Z. D. Bugarcic, Eur. J. Med. Chem. 2017, 142, 8-31. f) B. Bertrand, A. Casini, Dalton Trans., 2014, 43 , 4209-4219.

9 a) A. Zamora, G. Vigueras, V. Rodríguez, M. D. Santana, J. Ruiz, Coord. Chem. Rev. 2018, 360, 34–76. b) Z. Liu, P. J. Sadler, Acc. Chem. Res. 2014, 47, 1174-1185. c) Z. Liu, A. Habtemariam, A. M. Pizarro, S. A. Fletcher, A. Kisova, O. Vrana, L. Salassa, P. C. A. Bruijnincx, G. J. Clarkson, V. Brabec, P. J. Sadler, J. Med. Chem. 2011, 54, 3011-3026. d) V. Venkatesh, R. Berrocal-Martin, C. J. Wedge, I. Romero-Canelon, C. Sanchez-Cano, J. Song, J. P. C. Coverdale, P. Zhang, G. J. Clarkson, A. Habtemariam, S. W. Magennis, R. J. Deeth, P. J. Sadler, Chem. Sci., 2017, 8 , 8271–8278.

10 B. Dominelli, J. D. G. Correia, F. E. Kuehn, J. Organomet. Chem. 2018, 866, 153-164.

11 a) M. Galanski, B. K. Keppler, Anticaner. Agents. Med. Chem. 2007, 7, 55–73. b) C. Caporale, M. Massi, Coord. Chem. Rev. 2018, 363, 71-91. c) B. Dominelli, J. D. G. Correia, F. E. Kuehn, J. Organomet. Chem. 2018, 866, 153-164. d) G. Suss-Fink, J. Organomet. Chem. 2014, 751, 2-19.

12 a) Z. H. Siddik, Oncogene 2003, 22, 7265–7279. b) B. S. Murray, M. V. Babak, C. G. Hartinger, P. J. Dyson, Coord. Chem. Rev. 2016, 306, 86–114. c) C. Scolaro, A. Bergamo, L. Brescacin, R. Delfino, M. Cocchietto, G. Laurenczy, T. J. Geldbach, G. Sava, P. J. Dyson, J. Med. Chem. 2005, 48, 4161 – 4171. d) S. Ahmad, Polyhedron 2017, 138, 109–124. e) Z. Liu, P. J. Sadler, Acc. Chem. Res. 2014, 47, 1174-1185. f) Z. Adhireksan, G. E. Davey, P. Campomanes, M. Groessl, C. M. Clavel, H. Y., A. A. Nazarov, C. H. Fang Yeo, W. H. Ang, P. Dröge, U. Rothlisberger, P. J. Dyson, C. A. Davey, Nat. Commun. 2014, 5, 3462.

13 A. Levina, D. C. Crans, P. A. Lay, Coord. Chem. Rev. 2017, 352, 473–498.

14 H. S. Oberoi, N. V. Nukolova, A. V. Kabanov, T. K. Bronich, Adv. Drug Delivery Rev. 2013, 65, 1667–1685.

15 W. Kaim, B. Schwederski, A. Klein, "Bioinorganic Chemistry: Inorganic Elements in the Chemistry of Life", 2nd Edition, Wiley 2013.

16 a) A. Pilon, P. Gírio, G. Nogueira, F. Avecilla, H. Adams, J. Lorenzo, M. H. Garcia, A. Valente, J. Organomet. Chem. 2017, 852, 34-42. b) P. R. Florindo, D. M. Pereira, P. M. Borralho, C. M. P. Rodrigues, M. F. M. Piedade, A. C. Fernandes, J. Med. Chem. 2015, 58, 4339-4347. c) A. Valente, A. M. Santos, L. Côrte-Real, M. P. Robalo, V. Moreno, M. Font-Bardia, T. Calvet, J. Lorenzo, M. H. Garcia, J. Organomet. Chem. 2014, 756, 52-60.

17 W. A. Wani, U. Baig, S. Shreaz, R. A. Shiekh, P. F. Iqbal, E. Jameel, A. Ahmad, S. H. Mohd-Setapar, M. Mushtaque, L. T. Hun, New J. Chem., 2016, 40 , 1063-1090.

18 a) M. Patra, G. Gasser, Nat. Rev. Chem. 2017, 1, 1-12. b) S. S. Braga, A. M. S. Silva, Organometallics 2013, 32, 5626-5639.

19 a) G. Jaouen, A. Vessières, S. Top, Chem. Soc. Rev. 2015, 44, 8802-8817. b) Y. Wang, P. M. Dansette, P. Pigeon, S. Top, M. J. McGlinchey, D. Mansuy, G. Jaouen, Chem. Sci., 2018, 9, 70–78.

20 Y. Wang, M.-A. Richard, S. Top, P. M. Dansette, P. Pigeon, A. Vessières, D. Mansuy, G. Jaouen, Angew. Chem. Int. Ed. 2016, 55, 10431-10434.

21 O. Buriez, J. M. Heldt, E. Labb, A. Vessières, G. Jaouen, C. Amatore, Chem. Eur. J. 2008, 14, 8195-8203.

22 a) M. E. García, D. García-Vivó, A. Ramos, M. A. Ruiz, Coord. Chem. Rev. 2017, 330, 1–36. b) L. Busetto, P. M. Maitlis, V. Zanotti, Coord. Chem. Rev. 2010, 254, 470–486.

23 See for instance: a) P. Lang, M. Schwalbe, Chem. Eur. J. 2017, 23, 17398-17412. b) K. P. Chiang, S. M. Bellows, W. W. Brennessel, P. L. Holland, Chem. Sci. 2014, 5, 267-274. c) J. P. McInnis, M. Delferro, T. J. Marks, Acc. Chem. Res. 2014, 47, 2545-2557. d) G.-H. Huang, J.-M. Li, J.-J. Huang, J.-D. Lin, G. J. Chuang, Chem. Eur. J. 2014, 20, 5240-5243. e) B. S. Natinsky, C. Liu, Nat. Chem. 2019, 11, 199-203.

24 [FeFe]-Hydrogenase, K. D Swanson, D. O. Ortillo, J. B. Broderick, J. W. Peters, Encyclopedia of Inorganic and Bioinorganic Chemistry, 2011, Wiley, 2nd edition.

25 Selected references: a) F. Marchetti, Eur. J. Inorg. Chem. 2018, 3987–4003, and references therein. b) P. Tong, D. Yang, Y. Li, B. Wang, J. Qu, Organometallics 2015, 34, 3571−3576. c) Y. Chen, L. Liu, Y. Peng, P. Chen, Y. Luo, J. Qu, J. Am. Chem. Soc. 2011, 133, 1147-1149. d) J. He, C.-L. Deng, Y. Li, Y.-L. Li, Y. Wu, L.-K. Zou, C. Mu, Q. Luo, B. Xie, J. Wei, Organometallics 2017, 36, 1322-1330. e) A. Boni, T. Funaioli, F. Marchetti, G. Pampaloni, C. Pinzino, S. Zacchini, Organometallics 2011, 30, 4115-4122. f) M. A. Alvarez, M. E. García, R. González, M. A. Ruiz, Organometallics 2013, 32, 4601-4611.

26 G. Agonigi, M. Bortoluzzi, F. Marchetti, G. Pampaloni, S. Zacchini, V. Zanotti, Eur. J. Inorg. Chem. 2018, 960–971.

27 a) V. G. Albano, L. Busetto, F. Marchetti, M. Monari, S. Zacchini and V. Zanotti, Organometallics, 2003, 22, 1326-1331. b) V. G. Albano, L. Busetto, F. Marchetti, M. Monari, S. Zacchini, V. Zanotti, J. Organomet. Chem., 2004, 689, 528–538.

28 a) L. Busetto, F. Marchetti, S. Zacchini, V. Zanotti, E. Zoli, J. Organomet. Chem. 2005, 690, 348–357. b) V. G. Albano, L. Busetto, F. Marchetti, M. Monari, S. Zacchini, V. Zanotti, Z. Naturforsch. 2007, 62b, 427-438.

29 Recent references include: a) K. Chai, W. Kuang, Z. Lan, L. Zhang, Y. Jiang, T. Han, J. Niu, J. Wang, X. Duan, J. Inorg. Biochem. 2019, 192, 17-24. b) O. A. Lenis-Rojas, M. P. Robalo, A. I. Tomaz, A. Carvalho, A. R. Fernandes, F. Marques, M. Folgueira, J. Yáñez, D. Vázquez-García, M. López Torres, A. Fernández, J. J. Fernández, Inorg. Chem. 2018, 57, 13150-13166. c) H. Zhang, L. Guo, Z. Tian, M. Tian, S. Zhang, Z. Xu, P. Gong, X. Zheng, J. Zhao, Z. Liu, Chem. Commun. 2018, 54, 4421-4424. d) J. Castro, E. Manrique, M. Bravo, M. Vilanova, A. Benito, X. Fontrodona, M. Rodríguez, I. Romero, J. Inorg. Biochem. 2018, 182, 124-132. e) T. T. Fong, C. N. Lok, C. Y. Chung, Y. M. Fung, P. K. Chow, P. K. Wan, C. M. Che, Angew. Chem. Int. Ed. 2016, 55, 11935-11939.

30 G. Ciancaleoni, S. Zacchini, V. Zanotti, F. Marchetti, Organometallics 2018, 37, 3718−3731.

31 a) S. G. Eaves, D. S. Yufit, B. W. Skelton, J. A. K. Howard, P: J. Low, Dalton Trans., 2015, 44, 14341-14348. b) J. Ruiz, D. Sol, M. A. Mateo, M. Vivanco, Dalton Trans., 2018, 47, 6279–6282. c) V. G. Albano, S. Bordoni, L. Busetto, F. Marchetti, M. Monari, V. Zanotti, J. Organomet. Chem. 2003, 684, 37-43.

32 a) L. Busetto, V. Zanotti, J. Organomet. Chem. 2005, 690, 5430–5440. b) L. Busetto, P. M. Maitlis, V. Zanotti, Coord. Chem. Rev. 2010, 254, 470–486.

33 a) F. Marchetti, S. Zacchini, V. Zanotti, Chem. Commun., 2015, 51, 8101-8104. b) R. Mazzoni, F. Marchetti, A. Cingolani, V. Zanotti, Inorganics 2019, 7, 25.

34 a) T. Rundlöf, M. Mathiasson, S. Bekiroglu, B. Hakkarainen, T. Bowden, T. Arvidsson, J. Pharm. Biomed. Anal. 2010, 52, 645–651. b) L. Biancalana, L. K. Batchelor, T. Funaioli, S. Zacchini, M. Bortoluzzi, G. Pampaloni, P. J. Dyson, F. Marchetti, Inorg. Chem. 2018, 57, 6669−6685.

35 For a comparative view of solubility values of KCl respectively in H_2O and D_2O see: A. A. Sunler, J. Baumbach, J. Chem. Engineering Data, 1976, 21, 335-336.

36 a) J. Zhao, S. Gou, F. Liu, Chem. Eur. J. 2014, 20, 15216-15225. b) R. Gust, R. Krauser, B. Schmid, H. Schönenberger, Inorg. Chim. Acta 1996, 250, 203-218. c) R. Gust, R. Krauser, B. Schmid, H. Schönenberger, Arch. Pharm. Pharm. Med. Chem. 1998, 27-35.

37 Solubility of cisplatin in H_2O is estimated to be 3 $g \cdot L^{-1}$ [4e].

38 F. Marchetti, S. Zacchini, V. Zanotti, Organometallics 2018, 37, 107−115.

39 G. Agonigi, G. Ciancaleoni, T. Funaioli, S. Zacchini, F. Pineider, C. Pinzino, G. Pampaloni, V. Zanotti, F. Marchetti, Inorg. Chem. 2018, 57, 15172−15186.

40 W. G. Kirlin, J. Cai, S. A. Thompson, D. Diaz, T. J. Kavanagh, D. P. Jones, Free Rad. Biol. Med., 1999, 27, 1208–1218.

41 a) L. Busetto, F. Marchetti, S. Zacchini, V. Zanotti, Organometallics 2005, 24, 2297-2306. b) L. Busetto, F. Marchetti, M. Salmi, S. Zacchini, V. Zanotti, Eur. J. Inorg. Chem. 2008, 2437–2447. c) F. Marchetti, S. Zacchini, V. Zanotti, Eur. J. Inorg. Chem. 2012, 2456–2463.

42 V. G. Albano, L. Busetto, F. Marchetti, M. Monari, S. Zacchini, V. Zanotti, J. Organomet. Chem. 2006, 691, 4234–4243.

43 IR spectro-electrochemical experiments could not be satisfyingly carried out in aqueous medium, due to limited solubility and restricted IR spectral window.

44 B. S. Murray, L. Menin, R. Scopelliti, P. J. Dyson, Chem. Sci., 2014, 5, 2536-2545.

45 H. Chen, J. A. Parkinson, R. E. Morris, P. J. Sadler;J. Am. Chem. Soc., 2003, 125, 173.

46 S. P. Sau, P. Kumar, P. K. Sharma, P. J. Hrdlicka, Nucleic Acids Res., 2012, 1–9.

47 a) R. F. S. Lee, L. Menin, L. Patiny, D. Ortiz, P. J. Dyson; Anal. Chem., 2017, 89, 11985-11989. b) A. Levina, D. C. Crans, P. A. Lay, Coord. Chem. Rev. 2017, 352, 473–498. c) L. Biancalana, A. Pratesi, F. Chiellini, S. Zacchini, T. Funaioli, C. Gabbiani, F. Marchetti, New J. Chem., 2017, 41, 14574-14588.

48 F°/F = ratio between fluorescence value at the zero addition and at the i-th addition of the quencher; K_{SV} =Stern-Volmer constant see Table S3 in the Supporting Information); [Q] = total molar concentration of quencher [Q] = $C_{compound}$)

49 P. D. Ross, S. Subramanian, Biochemistry, 1981, 20, 3096–3102.

50 V. G. Albano, L. Busetto, F. Marchetti, M. Monari, S. Zacchini, V. Zanotti, J. Organomet. Chem. 2005, 690, 837–846.

51 F. Menges, "Spectragryph - optical spectroscopy software", Version 1.2.5, @ 2016-2017, http://www.effemm2.de/spectragryph.

52 G. R. Fulmer, A. J. M. Miller, N. H. Sherden, H. E. Gottlieb, A. Nudelman, B. M. Stoltz, J. E. Bercaw, K. I. Goldberg, Organometallics 2010, 29, 2176–2179.

53 W. Willker, D. Leibfritz, R. Kerssebaum, and W. Bermel, Magn. Reson. Chem., 1993, 31, 287-292.

54 N. M. Rice, H. M. N. H. Irving, M. A. Leonard, Pure & Appl. Chem. 1993, 65, 2373-2396.

55 M. Gross, J. Jordan, Voltammetry At Glassy Carbon Electrodes, Pure & Appl. Chem., 1984, 56, 1095-1129.

56 M. Krejčik, M. Daněk and F. Hartl, J. Electroanal. Chem. 1991, 317, 179-187.

57 G. M. Sheldrick, SADABS-2008/1 - Bruker AXS Area Detector Scaling and Absorption Correction, Bruker AXS: Madison, Wisconsin, USA, 2008

58 G. M. Sheldrick, ActaCrystallogr. C, 2015, 71, 3.

59 T. Mosmann, J. Immunol. Methods 1983, 65, 55-63.

60 A.R. Rosenkranz, S. Schmaldienst, K. M. Stuhlmeier, W. Chen, W. Knapp, G. J. Zlabinger, J. Immunol. Methods 1992, 156, 39–45.

61 T. Biver, F. Secco, M. R. Tinè, M. Venturini, A. Bencini, A. Bianchi, C. Giorgi, J. Inorg. Biochem. 2004, 98, 1531-1538.

62 G. Felsenfeld, S. Z.Hirschman, J. Mol. Biol. 1965, 13, 407-427.

63 M. J. Waring, J. Mol. Biol. 1965, 13, 269-282.

64 S. C. Gill, P. H. von Hippel, Anal. Biochem. 1989, 182, 319-326.